

Fundamental-measure free-energy density functional for hard spheres: Dimensional crossover and freezing

Y. Rosenfeld,^{1,*} M. Schmidt,² H. Löwen,^{2,†} and P. Tarazona³

¹*H.H. Wills Physics Laboratory, Bristol University, Royal Fort, Tyndall Avenue, Bristol BS8 1TL, United Kingdom*

²*Institut für Theoretische Physik II, Heinrich-Heine Universität Düsseldorf, Universitätsstrasse 1, 40225 Düsseldorf, Germany*

³*Departamento de Física de la Materia Condensada (C-XII), Universidad Autónoma de Madrid, E-28049 Madrid, Spain*

(Received 5 August 1996)

A geometrically based fundamental-measure free-energy density functional unified the scaled-particle and Percus-Yevick theories for the hard-sphere fluid mixture. It has been successfully applied to the description of simple (“atomic”) three-dimensional (3D) fluids in the bulk and in slitlike pores, and has been extended to molecular fluids. However, this functional was unsuitable for fluids in narrow cylindrical pores, and was inadequate for describing the solid. In this work we analyze the reason for these deficiencies, and show that, in fact, the fundamental-measure geometrically based theory provides a free-energy functional for 3D hard spheres with the correct properties of dimensional crossover and freezing. After a simple modification of the functional, as we propose, it retains all the favorable $D=3$ properties of the original functional, yet gives reliable results even for situations of extreme confinements that reduce the effective dimensionality D drastically. The modified functional is accurate for hard spheres between narrow plates ($D=2$), and inside narrow cylindrical pores ($D=1$), and it gives the exact excess free energy in the $D=0$ limit (a cavity that cannot hold more than one particle). It predicts the (vanishingly small) vacancy concentration of the solid, provides the fcc hard-sphere solid equation of state from closest packing to melting, and predicts the hard-sphere fluid-solid transition, all in excellent agreement with the simulations. [S1063-651X(97)07404-7]

PACS number(s): 61.20.Gy, 64.10.+h

I. INTRODUCTION

The applications of the density functional formalism are wide ranging: from quantum mechanical electronic calculations in metals, semiconductors, and insulators [1] to phase transitions and interfacial problems [2,3] of classical liquids. In particular, the density functional theory provides a microscopic theory for adsorption and wetting phenomena for both charged and neutral fluid systems. Most of the classical density functionals start from the bulk fluid state where the equation of state and pair correlation functions are known [4] and investigate then the inhomogeneous fluid subject to an external potential, e.g., a gravitational field or walls confining the system and inducing a layering in the homogeneous bulk fluid. Different kinds of confinement are conceivable; in particular, three of them are important which effectively reduce the dimensionality of the three-dimensional bulk fluid. First let us consider two parallel walls with a spacing of several intermolecular distances. By varying the plate distance one can continuously interpolate between two and three dimensions. Second, an even more dramatic confinement is given by a cylindrical pore [5]: By shrinking the pore size towards molecular spacing one can effectively reduce the dimensionality of the fluid from three to one. Third, by shrinking the size of a spherical cavity until it can hold at most one particle, one can reduce the effective dimensional-

ity of the fluid from three to zero.

These spatial confinements drastically affect structural and dynamical quantities as well as the location of phase transitions. The density profile exhibits sharp peaks corresponding to microscopic layers of the liquid, the viscosity is observed to increase drastically [6], and the location of the freezing transition [7,8], the glass transition [9], the critical point [10], and the triple point [11] significantly shift with respect to their bulk values. While it is difficult to prepare smooth well-defined walls for molecular liquids, it is relatively easy to confine mesoscopic colloidal suspensions between glass plates and in glassy tubes. The further advantage one gains in dealing with mesoscopic dispersions is that one can directly watch their positions and correlations in real space by using videomicroscopy. Suspensions confined between two glass plates were intensely investigated in recent years [12–18] and there are also some recent investigations for colloids in slit pores [19].

In principle, the exact three-dimensional (3D) free energy functional (if it was available) should be able to provide a unifying description of all such confined situations within density functional theory. The main aim of this paper is to present an approximate free-energy functional that features reliable crossover properties between effective dimensionalities. Basically the idea is as follows: Suppose we are starting with the exact density functional in three dimensions and we then reduce the dimensionality of the system by applying confining external potentials as walls and cylindrical pores. Then the exact three-dimensional functional reduces to the exact two-dimensional and one-dimensional functionals (respectively). Upon freezing, in the surface or in the bulk, the density profile has “zero-dimensional” characteristics, when every particle is practically confined to a cage (or a cavity

*On leave from the Nuclear Research Center Negev, Beer-Sheva, Israel.

†Also at Institut für Festkörperforschung, Forschungszentrum Jülich, D-52425 Jülich, Germany.

defined by its neighbors) which cannot contain more than one particle. In practice, however, the exact functional is not known. Hence the requirement to get a realistic lower-dimensional functional by shrinking the dimensionality of the system is an important consistency check of any approximate functional. This consistency is of particular importance if the 3D functional is invoked to describe situations of extremely confined fluids [20,5].

A relatively simple and the almost canonical starting point for classical fluids is the system of hard spheres. A hard-sphere fluid exhibits a freezing transition into a fcc solid for high enough packing fraction. The bulk structure factors are well known in the fluid for arbitrary densities [4]. Density profiles of inhomogeneous situations involving a single planar hard wall [21], two parallel hard walls [22,23,20,8], or a gravitational field [24] are well known. Therefore the inhomogeneous hard-sphere fluid is considered to be an important situation to test the validity of density functional approximations. In two dimensions, the hard-disk fluid is also well studied and for the one-dimensional hard rods even the exact free-energy functional is known [25], which provides a very important paradigm [26] for developing model free-energy functionals. Hence the hard-sphere fluid represents a convenient reference fluid where the crossover between different dimensionalities starting from the 3D functional should be tested explicitly.

When the free energy is expressed as a functional of the average one-body densities $\{\rho_i(\mathbf{r})\}$, of the various species $\{i\}$ of particles, all the relevant thermodynamic functions can be calculated. The central quantity is the excess free energy (over the exactly known “ideal-gas” contributions), $F_{\text{ex}}[\{\rho_i(\mathbf{r})\}]$, which originates in interparticle interactions. The performance of a 3D functional in quasi-2D and quasi-1D situations can be inferred from its ability to provide accurate description of the corresponding uniform (bulk) 2D and 1D fluids, respectively. The ability of the functional to stabilize a solid, and to predict a freezing transition, can be inferred from its result for the quasi-0D limit. The minimal prerequisite from the 3D functional, to have at least gross similarity to the exact values in lower effective dimensionality situations, was achieved [27,5] by the smoothed density approximation [27]. Many functionals of comparable, sometimes better, accuracy were subsequently developed [3], which could provide qualitative, sometimes quantitative, agreement with simulated density profiles of confined fluids. Most of these functionals were also able to exhibit a freezing transition for the hard spheres, which essentially requires only that the functional is finite in the 0D limit described below. They gave melting and freezing densities in reasonable, sometimes excellent, agreement [28,29] with simulations, but they had to assume *a priori* no vacancies in the solid. The correct Lindemann parameter of the solid near melting was sometimes obtained [29], but with incorrect density profiles. None of these functionals could feature the exact 0D limit, or the exact bulk-1D [25] limit. Functionals built upon the bulk-3D data as essentially numerical input do not contain the building blocks for achieving these limits.

The fundamental-measure free-energy model [30–35], on the other hand, is an approximation that enables derivation of the uniform (bulk) fluid properties as a special case, rather than employing them as input. The simplest such functional

[31] proved successful for 3D fluids in the bulk or in slitlike pores, but it was unsuitable for narrow cylindrical pores and unable to describe the solid. Yet, since it is built upon a well-defined set of geometric basis functions, it is possible to analyze it, term by term, to reveal its crossover properties, and then to improve its form so that it yields accurately even the freezing transition. We reemphasize that it is relatively easy to construct functionals specifically for 2D and 1D systems [see, e.g., Eqs. (14) and (15) below], but having a functional for 3D that works in arbitrary situations ranging from 0D to 3D is much more demanding.

In this work we show that, in fact, the fundamental-measure geometrically based theory [30–35] provides a free-energy functional for 3D hard spheres with the correct properties of dimensional crossover and freezing. A particular simple modification of the original functional is proposed which retains all the favorable $D=3$ properties of the original functional, but gives reliable results even for situations of extreme confinements that reduce the effective dimensionality D drastically. It is accurate for hard spheres between narrow plates ($D=2$), and inside narrow cylindrical pores ($D=1$), and gives the exact excess free energy in the $D=0$ limit (a cavity that cannot hold more than one particle). It predicts the (vanishingly small) vacancy concentration of the solid, provides the fcc hard-sphere solid equation of state in excellent agreement with the simulations from closest packing to melting, and predicts the hard-sphere fluid-solid transition in excellent agreement with the simulations.

In Sec. II we briefly review the geometrically based fundamental-measure free-energy functionals. The quasi-2D and quasi-1D limits are considered in Sec. III, while in Sec. IV we investigate the quasi-0D limit of the 3D functionals. In Sec. V we discuss the hard-sphere solid and the freezing transition as predicted by the functionals. The results are discussed in Sec. VI. In order not to interrupt the discussions with too much algebra, the essential details of our calculations are given in Appendixes A–E. A short account of the present work was published elsewhere [36].

II. GEOMETRICALLY BASED FUNDAMENTAL-MEASURE FREE-ENERGY FUNCTIONALS

The fundamental-measure free-energy density functional, which is being developed in recent years [30–35], keeps the geometric features to the forefront. It can be formulated *a priori* for mixtures of nonspherical molecules, and can derive the uniform fluid properties as a special case, rather than employ them as input. The basic idea is to interpolate between the “ideal-liquid” [37], high density, limit where the pair direct correlation function is dominated by convolutions of single-particle geometries, i.e., overlap volume and overlap surface area, and the limit of low density where it is given by the pair exclusion volume. The key for the realization of this idea is the convolution decomposition of the excluded volume for a pair of convex hard bodies in terms of characteristic functions for the geometry of the two individual bodies. On the basis of a unique convolution decomposition for spheres it was possible to derive [31] a fundamental-measure free-energy functional for hard sphere

mixtures, in which the weight functions represent the geometry of the individual particles. Starting with the excess free-energy functional for hard-spheres it was shown that the fundamental-measure *bridge* functional, which is derived from the free-energy functional, can then be successfully utilized for *arbitrary* pair interactions [34,30]. ‘‘Universality of the bridge functions’’ [38], which initiated a successful theory of the bulk fluid, is thus replaced by ‘‘universality of the bridge functional’’ [34,30], as a working hypothesis for both uniform and nonuniform classical fluids. The direct extension of the functional to molecular (‘‘complex’’) fluids is made possible by the relation of the convolution decomposition for spheres and the Gauss-Bonnet theorem for convex bodies.

The fundamental-measure excess free-energy functional for hard-sphere mixtures of dimensionality D was postulated [31] to have the form

$$\frac{F_{\text{ex}}[\{\rho_i(\mathbf{r})\}]}{k_B T} = \int d\mathbf{x} \Phi[\{n_\alpha(\mathbf{x})\}], \quad (1)$$

where it is assumed that the *excess free-energy density* Φ is a function of only the system averaged fundamental geometric measures of the particles,

$$n_\alpha(\mathbf{x}) = \sum_i \int \rho_i(\mathbf{x}') w_i^{(\alpha)}(\mathbf{x} - \mathbf{x}') d\mathbf{x}'. \quad (2)$$

The *weight functions* $w_i^{(\alpha)}$ are characteristic functions for the geometry of the particles, and are obtained from the convolution decomposition of the excluded volume for a pair of particles in terms of characteristic functions for the geometry of the individual particles. This form implies that the n -particle direct correlation functions $c_{i_1, \dots, i_n}^{(n, \text{FD})}$, which are functional derivatives of $F_{\text{ex}}[\{\rho_i(\mathbf{r})\}]$, are given by convolutions of the geometric characteristic functions. In particular, the two-particle functions have the form

$$c_{i_1, i_2}^{(2, \text{FD})}(\mathbf{r}_1, \mathbf{r}_2) = - \int \sum_{\alpha, \beta} \Psi_{\alpha\beta}[\{n_\gamma(\mathbf{x})\}] w_{i_1}^{(\alpha)}(\mathbf{x} - \mathbf{r}_1) \times w_{i_2}^{(\beta)}(\mathbf{x} - \mathbf{r}_2) d\mathbf{x}, \quad (3)$$

where

$$\Psi_{\alpha\beta} = \Phi''_{\alpha\beta} = \frac{\partial^2 \Phi}{\partial n_\alpha \partial n_\beta} \quad (4)$$

as required by the scaled-field-particle [39] geometric analysis, and incorporating the basic idea to *interpolate* between the ‘‘ideal-liquid’’ [37] (high density) and ideal-gas limits. The ideal-liquid pair direct correlation function is dominated by convolutions of single-particle geometries, i.e., overlap volume and overlap surface area, and the low density direct correlation function is given by the pair exclusion volume. This interpolation is realized through the convolution decomposition of the excluded volume for a pair of convex hard bodies in terms of characteristic functions for the geometry of the two individual bodies. A *unique* solution was found

for the special case of spheres with a *convolution decomposition* involving a minimal number of different weight functions [31]:

$$-f_{ij}(\mathbf{r}_{ij}) = w_i^{(0)} \otimes w_j^{(3)} + w_j^{(0)} \otimes w_i^{(3)} + w_i^{(1)} \otimes w_j^{(2)} + w_j^{(1)} \otimes w_i^{(2)} - \mathbf{w}_i^{(V1)} \otimes \mathbf{w}_j^{(V2)} - \mathbf{w}_j^{(V1)} \otimes \mathbf{w}_i^{(V2)}, \quad (5)$$

where the Mayer function for a pair of spheres is minus the Heaviside step function,

$$f_{ij}(\mathbf{r}_{ij}) = -\Theta(R_i + R_j - r), \quad (6)$$

and where the convolution product,

$$w_i^{(\alpha)} \otimes w_j^{(\gamma)} = \int w_i^{(\alpha)}(\mathbf{x} - \mathbf{r}_i) \cdot w_j^{(\gamma)}(\mathbf{x} - \mathbf{r}_j) d\mathbf{x}, \quad (7)$$

also implies the scalar product between vectors. The weight-function space for $D \geq 1$ contains at least three functions, two scalar functions representing the characteristic functions for the volume and the surface of a particle and a surface vector function,

$$w_i^{(D)}(r) = \Theta(R_i - r), \\ w_i^{(D-1)}(\mathbf{r}) = |\nabla w_i^{(D)}(r)| = \delta(R_i - r), \\ \mathbf{w}_i^{(D-1)}(\mathbf{r}) = -\nabla w_i^{(D)}(r) = \frac{\mathbf{r}}{r} \delta(R_i - r). \quad (8)$$

In 3D, the other weight functions are just proportional to these three, and are given by

$$w_i^{(0)}(\mathbf{r}) = \frac{w_i^{(2)}(\mathbf{r})}{4\pi R_i^2}, \quad w_i^{(1)}(\mathbf{r}) = \frac{w_i^{(2)}(\mathbf{r})}{4\pi R_i}, \\ \mathbf{w}_i^{(V1)}(\mathbf{r}) = \frac{\mathbf{w}_i^{(V2)}(\mathbf{r})}{4\pi R_i}. \quad (9)$$

The weighted densities $n_\alpha(\mathbf{x})$ are *dimensional* quantities with dimensions $[n_\alpha] = (\text{volume})^{(\alpha-D)/D}$ where $0 \leq \alpha \leq D$, and provide a functional basis set $\{\varphi_j\}$ for expanding the function

$$\Phi = \sum_i A_i(n_D) \varphi_i, \quad (10)$$

of dimension $(\text{volume})^{-1}$. The coefficients, $A_i(n_D)$, as functions of the dimensionless n_D , are determined from the scaled-particle differential equation,

$$-\Phi + \sum_\alpha n_\alpha \frac{\partial \Phi}{\partial n_\alpha} + n_0 = \frac{\partial \Phi}{\partial n_D}, \quad (11)$$

and the constants of integration can be fixed by known limits or desirable properties. By including only the following positive power combinations of the weighted densities:

$$\{\varphi_j\} = n_0, n_1 n_2, \mathbf{n}_{V1} \cdot \mathbf{n}_{V2}, n_2^3, n_2(\mathbf{n}_{V2} \cdot \mathbf{n}_{V2}), \quad (12)$$

the following *simplest* 3D excess free-energy density was derived [31,34]:

$$\begin{aligned}\Phi^{(D=3)}[\{n_\alpha\}] &= \Phi_1^{(3)} + \Phi_2^{(3)} + \Phi_3^{(3)}, \\ \Phi_1^{(3)} &= -n_0 \ln(1 - n_3), \quad \Phi_2^{(3)} = \frac{n_1 n_2 - \mathbf{n}_{V1} \cdot \mathbf{n}_{V2}}{1 - n_3}, \\ \Phi_3^{(3)} &= \frac{\frac{1}{3} n_2^3 - n_2 (\mathbf{n}_{V2} \cdot \mathbf{n}_{V2})}{8\pi(1 - n_3)^2}.\end{aligned}\quad (13)$$

The notation \mathbf{n}_{V2} was chosen in order to emphasize that in general, $|\mathbf{n}_{V2}(\mathbf{x})| \neq n_2(\mathbf{x})$. This free-energy model provides a unified derivation of the Percus-Yevick [40] and scaled-particle [41] theories for hard spheres. The Percus-Yevick and scaled-particle theories provide the most comprehensive available analytic description of the bulk hard-sphere thermodynamics and structure, and serve as the standard input for weighted density models. Indeed, the ability to describe the Percus-Yevick direct correlations geometrically [39], in a form that relates to the scaled-particle thermodynamics, was essential for the derivation of the fundamental-measure functional. For the uniform 3D fluid, the resulting $c_{i_1, i_2}^{(2, \text{FD})}(r)$ is identical to the analytic solution of the Percus-Yevick equation as interpreted geometrically [39] by the scaled-field-particle diagrammatic description. It was subsequently found [42,43] that in the special case of 3D spheres the functional (13) is unique in the sense that a completely equivalent [44] functional can be derived, so that it contains only scalar weight functions (requiring, however, the inclusion of derivatives of the Dirac δ function). This equivalence is also important for checking numerical calculations: The calculations using this so-called ‘‘simplified’’ version are completely equivalent to using the original functional (13). The bulk three-particle direct correlation function was calculated in k space [31,42,44] with good agreement with simulations. The solution of the density profile equations (i.e., the Euler-Lagrange equations for minimizing the grand potential) using the functional (13), in the special case when the external potential is generated by a *test particle* at the origin of coordinates, yields [34,35] bulk pair correlation functions, which almost satisfy the Ornstein-Zernike relation with the Percus-Yevick direct correlation functions obtained from functional differentiation, yet are in even better agreement with the simulations. The functional (13) yields the Percus-Yevick bulk direct correlation functions, thus predicting that bulk hard-sphere fluid binary mixtures never phase separate. Yet in the test-particle bulk limit it predicts phase separation for large size ratios between the spheres [35]. The functional (13) yields density profiles of hard spheres and hard-sphere binary mixtures [34,43] in slitlike pores, in very good agreement with the simulations even for narrow slits.

The same procedure that led to the above 3D result, when applied [31] to one-dimensional ‘‘spheres,’’ leads to the exact result for hard rods as obtained earlier by Percus [25], and rewritten as

$$\Phi^{(D=1)}[\{n_\alpha\}] = \Phi_1^{(1)} = -n_0 \ln(1 - n_1). \quad (14)$$

In two dimensions it leads to [33]

$$\begin{aligned}\Phi^{(D=2)}[\{n_\alpha\}] &= \Phi_1^{(2)} + \Phi_2^{(2)}, \\ \Phi_1^{(2)} &= -n_0 \ln(1 - n_2), \quad \Phi_2^{(2)} = \frac{n_1 n_1 - \mathbf{n}_{V1} \cdot \mathbf{n}_{V1}}{4\pi(1 - n_2)},\end{aligned}\quad (15)$$

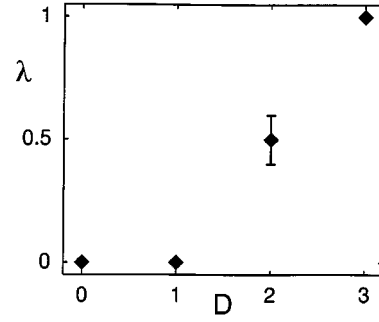


FIG. 1. Variation of the prefactor λ with the effective dimensionality of the fluid. The error bar for $D=2$ indicates a range of possible values (see the text).

which, with minor adjustments as required for an even dimensionality ($D=2 = \text{even}$), also provides accurate analytic structure factors for hard disks [33]. It should be emphasized that in both these 1D and 2D functionals, the weighted densities involve the characteristic functions for ‘‘spheres’’ of the corresponding dimensionality, namely, rods and disks, respectively.

Earlier discussion of the crossover behavior of the fundamental-measure functional [Eq. (13)] can now be recalled. The 2D limit of the 3D functional tightly bounds the exact hard-disk excess free energy from above [43,34]. The 1D limit of the 3D functional yields a nonintegrable singularity in the $\Phi_3^{(3)}$ contribution [43,34]. It was observed, however [34], that without the $\Phi_3^{(3)}$ term, the 1D limit of the 3D functional yields the *exact* excess free energy of the bulk hard-rod system. Moreover [34], without the $\Phi_3^{(3)}$ term the 2D limit of the 3D functional tightly bounds the exact hard-disk excess free energy from below. In addition, it was found [34] that the 1D limit of the 2D functional provides an excellent approximation to the exact 1D bulk excess free energy. Thus the 3D functional [Eq. (13)] without the $\Phi_3^{(3)}$ term and the 2D functional [Eq. (15)] give comparable results for the 2D (hard disks) and 1D (hard rods) uniform hard-sphere fluids. It was clear [34] from all these results that as the effective dimensionality of the system is smaller than $D=2$, then the contributions of the $\Phi_3^{(3)}$ term should gradually diminish. The crossover behavior of the fundamental-measure functionals requires ‘‘switch off’’ of nonintegrable singularities as the dimensionality decreases, clearly seen by comparing the forms Eqs. (13)–(15) of the free-energy density functions. This mechanism should eventually be built into the theory by modifying the form of the $\Phi_3^{(3)}$ term in Eq. (13), i.e., by enlarging the set $\{\varphi_j\}$ of basis forms. At present we still do not have a guiding principle that will *uniquely* determine the optimal basis set $\{\varphi_j\}$. We hope that by *detailed* analysis of the behavior of the different components in the functional, in extreme confinements, we shall be able to systematically improve the simplest functional (13), and eventually find the optimal form. In order to facilitate the discussion we introduce the prefactor λ (see Fig. 1) multiplying the third term in Eq. (13), as a function of the effective dimensionality, i.e., $\lambda(D_{\text{eff}})$, and consider the λ -dependent excess free-energy density:

$$\Phi^{(D=3)}[\{n_\alpha\}; \lambda] = \Phi_1^{(3)} + \Phi_2^{(3)} + \lambda \Phi_3^{(3)}. \quad (16)$$

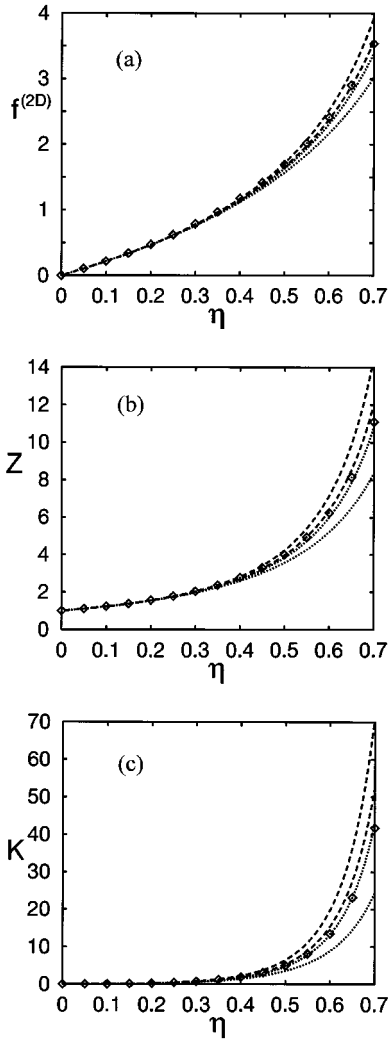


FIG. 2. (a) Excess free energy for hard disks, $f_{\text{ex}}^{(2D)}$, as a function of the packing fraction η . (b) Compressibility factor $Z^{(2D)} = 1 + \eta \partial f_{\text{ex}}^{(2D)} / \partial \eta$. (c) Second derivative (“compressibility”) $K = \eta^2 \partial^2 f_{\text{ex}}^{(2D)} / \partial \eta^2$. The lines from top to bottom correspond to $\lambda = 1, 0.6, 0.4, 0$ in Eq. (A14). The points represent the scaled-particle equation of state, which is highly accurate [54].

III. QUASI-2D AND QUASI-1D LIMITS OF THE 3D FUNCTIONAL

A. Excess free energy for additive hard disks

Consider the 3D hard-sphere functional [Eq. (13)] for a one-component hard-sphere system in slab geometry, in the “2D limit” of the density profiles, $\rho(\mathbf{r}) = \rho(z) = \rho^{(2D)} \delta(z)$, where $\rho^{(2D)} = N/A$ is the 2D density, and $\eta = \rho^{(2D)} \pi R^2$ is the 2D packing fraction. In this limit, $f^{(2D)} = F_{\text{ex}}[\{\rho(\mathbf{r})\}] / Nk_B T$ can be reduced to a single integral that can be performed analytically [43,34] [see Eq. (A14) in Appendix A]. We see from Fig. 1 in [34], as well as from our Fig. 2(a), that the exact 2D excess free energy is tightly bound by $f^{(2D)}$ with or without the contribution of $\Phi_3^{(3)}$, and that we can estimate (see Fig. 1): $\lambda(D_{\text{eff}}=2) = 0.4-0.6$. Any initial small difference between two functions is generally enhanced when taking the derivatives. Because of the weak λ dependence of $f^{(2D)}$ this choice is better appreciated by taking the first and second density derivatives of the free energies in Fig. 2(a), as

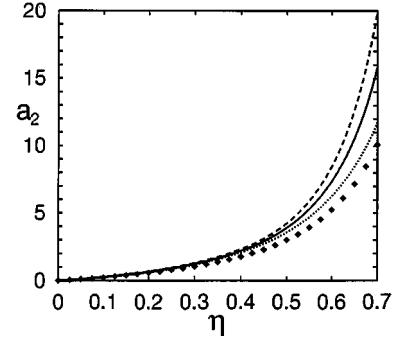


FIG. 3. Nonadditivity coefficient for hard disks (see Appendix C). Comparison of $a_{2,\text{exact}}^{(2D)}(\eta)$ as approximated by Eq. (B14) (diamonds), with $a_2(\lambda, \eta)$ for different values of λ (lines, from top to bottom $\lambda = 1, 0.5, 0$) for $\eta = 0.6$.

presented in Figs. 2(b) and 2(c). Similar reasoning applies also to functional derivatives, and the choice of λ should be sharpened by considering the pair direct correlations (see below).

B. Excess free energy for nonadditive hard disks

Following an idea in Ref. [43], consider a binary mixture of hard spheres with radius R in the 2D limit with densities $\rho_1(z) = \rho^{(2D)} \delta(z + \omega)$; $\rho_2(z) = \rho^{(2D)} \delta(z - \omega)$ where $2\rho^{(2D)} = N/A$ is the 2D density, and $\pi(2\rho^{(2D)})R^2 = \eta$ is the 2D packing fraction (Appendix B). This system is equivalent to an equimolar mixture of nonadditive hard disks with $R_{12} = [R^2 - \omega^2]^{1/2}$, with a *negative* nonadditivity parameter which, for small values of ω , is given by

$$\Delta \equiv 2(R_{12}/R - 1) \cong -(\omega/R)^2. \quad (17)$$

The function $f^{(2D)}(\lambda, \eta, \omega) = F_{\text{ex}}[\{\rho(\mathbf{r})\}; \lambda] / k_B T A$ can be calculated analytically (see Appendix C), and has the following expansion in powers of ω : $f^{(2D)}(\lambda, \eta, \omega) = f^{(2D)}(\lambda, \eta) + \lambda \eta^2 (\omega/R) + a_2(\lambda, \eta) [-(\omega/R)^2] + \dots$, where $a_2(\lambda=0, \eta) \neq 0$. Given the nonadditivity parameter Δ , the exact excess free energy for the 2D hard-disk fluid is expected to have the following expansion [45]; $f_{\text{exact}}^{(2D)}(\eta, \Delta) = f_{\text{exact}}^{(2D)}(\eta) + a_{2,\text{exact}}^{(2D)}(\eta) \Delta + \dots$, and we find (see Fig. 3) that $a_{2,\text{exact}}^{(2D)}(\eta) \cong \eta \partial f_{\text{exact}}^{(2D)}(\eta) / \partial \eta$ is comparable with $a_2(\lambda, \eta)$. However, the correct expansion type (i.e., without the $\lambda \eta^2 \omega$ term) is achieved only with $\lambda=0$. Otherwise, for $\lambda > 0$ we have $f^{(2D)}(\lambda, \eta, \omega) > f^{(2D)}(\lambda, \eta)$ for small values of ω , which is unphysical. Yet we find that, in terms of magnitude, $f^{(2D)}(\lambda \cong 0.5, \eta, \omega)$ still agrees well (see Fig. 4) with the expansion of $f_{\text{exact}}^{(2D)}(\eta, \Delta)$, for $-\Delta < \sim 0.1$. Moreover, $f^{(2D)}(\lambda, \eta, \omega = -R) = f^{(2D)}(\lambda, \eta/2, \omega = 0)$, which should be compared with the exact relation $f_{\text{exact}}^{(2D)}(\eta, \Delta = -1) = f_{\text{exact}}^{(2D)}(\eta/2, \Delta = 0)$.

Regarding this last result, we can make the general observation that the fundamental-measure picture guarantees that the above construction of nonadditive hard disks or hard rods, by considering two planes or two lines, respectively, should always give the result $f(\eta, \Delta = -1) = f(\eta/2, \Delta = 0)$, where $f(\eta, \Delta = 0)$ is the result of the same theory for the one-component system of additive disks or rods, respectively. In particular, since with $\lambda=0$ we obtain (Appendix C)

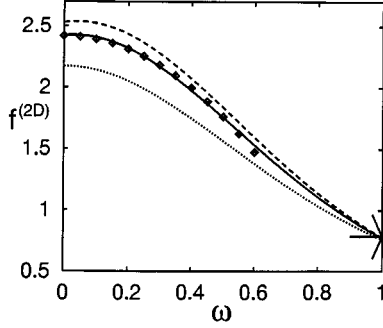


FIG. 4. Excess free energy for nonadditive hard disks (see Appendix C). Comparison of $f^{(2D)}(\lambda, \eta, \omega)$ for different values of λ (from top $\lambda=1, 0.7, 0$) with the expansion $f_{\text{SPT}}^{(2D)}(\eta, \Delta) = f_{\text{SPT}}^{(2D)}(\eta) + a_{2, \text{SPT}}^{(2D)}(\eta)\Delta$ (diamonds) for $\eta=0.6$. On the scale of the figure all lines and the continuation of the sequence of diamonds all meet at about the same point for $\omega=1$.

the exact $f^{(1D)}(\eta, \Delta=0) = -\ln(1-\eta)$, we thus also get the exact $f^{(1D)}(\eta, \Delta=1)$, and we interpolate accurately between $\Delta=0$ and $\Delta=1$.

C. Direct correlation functions for additive hard disks

The 2D limit of the pair direct correlation functions can also be reduced to a one-dimensional integration of explicitly given functions, but the final integral is evaluated numerically (see Appendix A). The contributions to $c^{(2, \text{FD})}(r)$, which are associated with the convolutions of two δ functions, contain a $1/r$ singularity. This singularity is canceled, however, in the terms that contribute to the pair direct correlation function of the uniform 3D fluid. The convolution terms related to $\Psi_{2, v_2} = \Psi_{v_2, 2} = -\lambda \mathbf{n}_{v_2} / 4\pi(1-n_3)^2$ (see Appendix A) have a singularity [46] which is not canceled out. But the vector weighted densities, and thus also Ψ_{2, v_2} and $\Psi_{v_2, 2}$, vanish in the uniform 3D limit, so that the singularity disappears anyway. The $1/r$ singularity, which remains, however, for the 2D (“hard-disk”) limit of the 3D functional, has a marked effect on the direct correlation function $c(r)$ (see Fig. 5). Yet, it is integrable, and we can get quite accurate structure factors (see Fig. 6), $S(k)$, for the hard-disk fluid if we take $\lambda=0.3$. If we discard the singular term, then with $\lambda=0.4$ we obtain good agreement with the

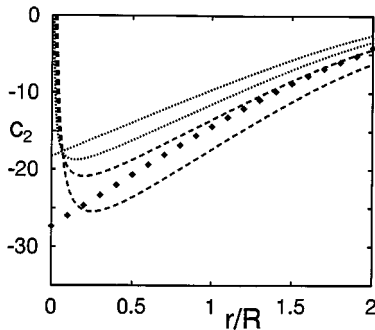


FIG. 5. Direct correlation function $c^{(2, \text{FD})}(r)$, for the hard disks at $\eta=0.6$. The lines from bottom to top correspond to $\lambda=1, 0.5, 0.24, 0$, in Eq. (A24). The points give the solution of the Percus-Yevick equation [47]. Compare with Fig. 3 in [33].

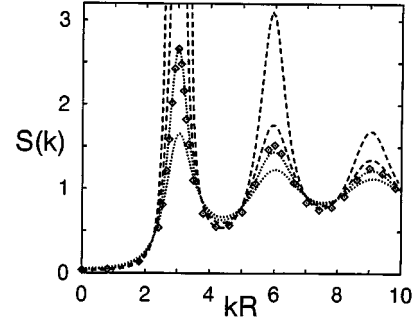


FIG. 6. Structure factor $S(k) = 1/[1 - \rho \tilde{c}^{(2, \text{FD})}(k)]$, for the hard disks at $\eta=0.6$. The lines from top to bottom near the first peak correspond to $\lambda=1, 0.5, 0.24, 0$. The points give the results of the analytic fundamental measure description developed in 2D [33]. Compare with Fig. 5 in [33].

numerical solution [47] of the Percus-Yevick equation for hard disks, for both $c(r)$ and $S(k)$. In either Fig. 6 (see also Fig. 7) or Fig. 8, the corresponding $S(k)$'s for $\lambda=1$ and $\lambda=0$ are significantly worse than those for $\lambda=0.4-0.6$, and the prefactor $\lambda(D_{\text{eff}}=2)=0.4-0.6$ is similar to that obtained above from considering the equation of state (see Fig. 1).

D. Excess free energy and direct correlation functions of hard rods

The 1D limit for the one-component system is obtained with the following density profile: $\rho(x, y) = \rho^{(1D)} \delta(x) \delta(y)$, where $\rho^{(1D)} = N/L$ is the number of spheres divided by the length of the line (i.e., the 1D density), and the 1D packing fraction is defined by $\eta = 2\rho^{(1D)}R$. In this limit the contribution from the third term diverges,

$$f_3^{(1D)} = \int \Phi_3^{(3)} d^3r \rightarrow -\infty. \quad (18)$$

Yet (see Appendix C), the limit for the excess free energy per particle without the contribution of the $\Phi_3^{(3)}$ term in Eq. (13) is the exact 1D result for the excess free energy $f^{(1D)} = F_{\text{ex}}/Nk_B T$:

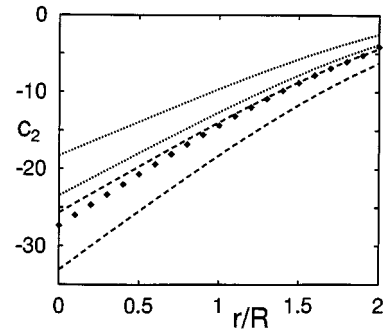


FIG. 7. Same as Fig. 5 but without the (singular) last term in Eq. (A26). The lines from bottom to top correspond to $\lambda=1, 0.5, 0.24, 0$.

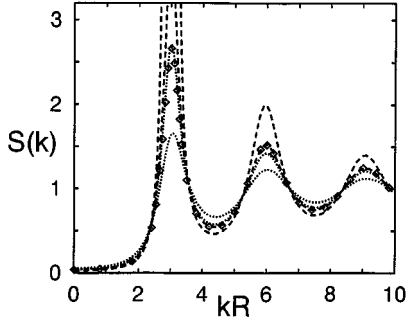


FIG. 8. Same as Fig. 6 but without the (singular) last term in Eq. (A26). The lines from top to bottom near the first peak correspond to $\lambda = 1, 0.5, 0.35, 0$.

$$f_{1+2}^{(1D)} = \frac{F_{\text{ex}}[\{\rho(\mathbf{r})\}; \lambda = 0]}{Nk_B T} = \int [\Phi_1^{(3)} + \Phi_2^{(3)}] d^3 r$$

$$= -\ln(1 - \eta). \quad (19)$$

Extending this calculation to evaluate the direct correlation function (see Appendix C), without the contribution of the $\Phi_3^{(3)}$ term, we find the remarkable result that

$$c^{(2,FD)}(r = |\mathbf{r}_1 - \mathbf{r}_2|; \lambda = 0) = \frac{-\eta}{(1 - \eta)^2} \left(1 - \frac{r}{2R}\right) - \frac{1}{1 - \eta}, \quad (20)$$

which is again *exact* for hard rods. Considering the required contribution of the $\Phi_3^{(3)}$ term in Eq. (13), relative to the full term, as a function of the effective dimensionality, i.e., $\lambda(D_{\text{eff}})$ in Eq. (16), we thus find that $\lambda(D_{\text{eff}} = 1) = 0$ eliminates the nonintegrable singularity of the free energy to yield the *exact* $f^{(1D)}$ and $c^{(2,FD)}(r)$ (see Fig. 1).

IV. QUASI-0D LIMIT OF THE 3D FUNCTIONAL

The quasi-0D situation for hard spheres of any dimensionality is achieved by an external potential such that there is a cavity which cannot hold more than one particle. Consider first the strict 0D limit, $\rho(\mathbf{r}) = \rho^{(0D)} \delta(\mathbf{r})$, where $\rho^{(0D)} = N = \eta \leq 1$ is also the 0D packing fraction. This is an asymptotic limit of the solid (see below) when considered as a superposition of δ functions. We now try to recover that limit as the ultimate crossover for any density functional. The exact $\Phi^{(D=1)}$ is directly integrated to give the exact $f^{(0D)}$ by a change of variables, $\tau = 1 - n_1(x)$ and $d\tau = -n_0(x)dx$. It is important to note that the same applies to the first term of the fundamental-measure functional, in any dimension, $\Phi_1^{(D)} = -n_0 \ln(1 - n_D)$, and in particular to $\Phi_1^{(2)}$ and $\Phi_1^{(3)}$, which have the same structure as the exact $\Phi^{(D=1)}$: Since for any D we have

$$w_i^{(D)}(r) = \Theta(R_i - r) \quad (21)$$

and

$$\Omega_D w_i^{(0)}(r) = w_i^{(2)}(r) = -\frac{dw_i^{(D)}(r)}{dr} = \delta(R_i - r), \quad (22)$$

where Ω_D is the surface area of the unit sphere, we make the important observation that when evaluating the 0D limit for hard spheres of any dimensionality, the $\Phi_1^{(D)}$ term yields the same result,

$$f^{(0D)} = \frac{F_{\text{ex}}[\{\rho(\mathbf{r})\}]}{k_B T} = \int d\mathbf{r} [-n_0 \ln(1 - n_D)]$$

$$= -\int_0^\infty \Omega_D r^{D-1} dr \eta w^{(0)}(r) \ln[1 - \eta w^{(D)}(r)]$$

$$= \eta + (1 - \eta) \ln(1 - \eta), \quad (23)$$

which is the *exact* 0D limit (see Appendix D). This provides additional justification for the validity of the geometric building blocks entering the fundamental-measure generalization, $\Phi^{(D)}$, of the exact 1D functional, $\Phi^{(D=1)}$.

Note that in the strict 0D limit, $\rho(\mathbf{r}) = \rho^{(0D)} \delta(\mathbf{r})$, the terms $n_{(D-1)} n_{(D-1)}$ and $\mathbf{n}_{V(D-1)} \cdot \mathbf{n}_{V(D-1)}$ become equal, and they diverge at $r = R$. However,

$$n_{(D-1)} n_{(D-1)} - \mathbf{n}_{V(D-1)} \cdot \mathbf{n}_{V(D-1)} = 0, \quad (24)$$

i.e., the ‘‘antisymmetric’’ form of both $\Phi_2^{(2)}$ and $\Phi_2^{(3)}$ cancels out exactly these diverging terms, and thus both $\Phi_2^{(2)}$ and $\Phi_2^{(3)}$ vanish. However, $\Phi_3^{(3)}$ does not possess such an anti-symmetry, and gives a strong negative divergence, $\int \Phi_3^{(3)} d^3 r \rightarrow -\infty$. From the point of view of Eq. (16) then the prefactor should be $\lambda(D_{\text{eff}} = 0) = 0$ (see Fig. 1).

A deeper insight into the functional may be obtained by considering the quasi-0D case, with $\rho(\mathbf{r})$ restricted to the inside of a spherical cavity of radius δ , where $\Delta = \delta/R \ll 1$. The exact $\Phi^{(D=1)}$ still gives the exact $f^{(0D)}$, but in 3D the volume integral of $\Phi_1^{(3)}$ differs from the exact $f^{(0D)}$ by a term of order Δ . At the same time, the cancellation by anti-symmetry of $\Phi_2^{(3)}$ becomes incomplete. Remarkably, its volume integral is exactly such that $f_{1+2}^{(0D)} = \int d\mathbf{r} [\Phi_1^{(3)} + \Phi_2^{(3)}]$ differs from the exact $f^{(0D)}$ only by a term of order Δ^2 . This makes clear that the first two terms in Eq. (13) fit properly in a hierarchical expansion, and the fundamental-measure forms, which were originally proposed for describing the fluid, provide the correct basis functions also in quasi-0D situations. Moreover, we attempted to find the exact third term in quasi-0D. We considered several radial forms (Appendix E) of $\rho(\mathbf{r}) = \rho(r)$ (step, parabolic, and Gaussian [48]) to find numerically (see Table I) that the difference from the exact 0D result was always $f^{(0D)} - f_{1+2}^{(0D)} = \int d\mathbf{r} [\Phi_{3,\text{exact-0D}}^{(3)}]$, where

$$\Phi_{3,\text{exact-0D}}^{(3)} = \left[\frac{\frac{1}{3} (n_2)^3}{8 \pi (1 - n_3)^2} \right] 3 \xi (1 - \xi)^2, \quad (25)$$

and $\xi(\mathbf{r}) \equiv |\mathbf{n}_{V2}(\mathbf{r})/n_2(\mathbf{r})|$. With $n_2 \sim \Delta^{-1}$, $1 - \xi \sim \Delta^2$, and the integral being extended over a shell width of order Δ , this gives a total contribution of order Δ^2 . However, the third term, $\Phi_3^{(3)}$, diverges as $-\Delta^{-2}$, and produces unbounded negative free energy for strongly localized density distributions. This explains why earlier studies [31,42,43] found the functional Eq. (13) to be unsuited for applications to freezing.

TABLE I. Contributions of the different terms in the free-energy functional, to the excess free energy in the quasi-0D limit, for a Gaussian density distribution $\rho(r) = \eta(\alpha/\pi)^{3/2}e^{-\alpha r^2}$ as a function of the occupancy η , for $\alpha=50$, as compared with the exact 0D excess free energy $f^{(0D)} = \eta + (1-\eta)\ln(1-\eta)$. We defined $f_1^{(0D)} = \int \Phi_1^{(3)} d^3r$, $f_2^{(0D)} = \int \Phi_2^{(3)} d^3r$, $\Delta f = f^{(0D)} - (f_1^{(0D)} + f_2^{(0D)})$, $f_3^{(0D)} = \int \Phi_{3,\text{exact-0D}}^{(3)} d^3r$. The numbers in brackets represent powers of 10.

η	$f^{(0D)}$	$f_1^{(0D)}$	$f_2^{(0D)}$	Δf	$\Delta f - f_3^{(0D)}$
0.999980[-1]	0.517533[-2]	0.398896[-2]	0.118424[-2]	0.212685[-5]	0.100472[-9]
0.199996[+0]	0.214843[-1]	0.164745[-1]	0.499071[-2]	0.190490[-4]	0.168709[-9]
0.299994[+0]	0.503254[-1]	0.383674[-1]	0.118852[-1]	0.727571[-4]	0.206725[-9]
0.399992[+0]	0.935005[-1]	0.708121[-1]	0.224906[-1]	0.197812[-3]	0.236631[-9]
0.499990[+0]	0.153419[+0]	0.115294[+0]	0.376746[-1]	0.450856[-3]	0.413538[-9]
0.599988[+0]	0.233473[+0]	0.173828[+0]	0.587140[-1]	0.930517[-3]	0.669544[-9]
0.699986[+0]	0.338791[+0]	0.249326[+0]	0.876409[-1]	0.182472[-2]	0.948285[-9]
0.799984[+0]	0.478087[+0]	0.346427[+0]	0.128112[+0]	0.354769[-2]	0.148643[-8]
0.899982[+0]	0.669700[+0]	0.474002[+0]	0.188392[+0]	0.730603[-2]	0.251677[-8]
0.999980[+0]	0.999764[+0]	0.662866[+0]	0.311892[+0]	0.250050[-1]	0.229100[-5]

V. THE HARD-SPHERE fcc SOLID AND THE FLUID-SOLID TRANSITION

Modeling the 3D solid by Gaussians, of width $1/\sqrt{\alpha}$, at fcc sites \mathbf{R}_i [27,28],

$$\rho(\mathbf{r}) = \eta_0 \sum_i \left(\frac{\alpha}{\pi} \right)^{3/2} e^{-\alpha(\mathbf{r}-\mathbf{R}_i)^2}, \quad (26)$$

the solution of the density profile equations, by minimization of the grand potential, gives the optimal parameter α for a given total average density of the system. We found that the contribution of $[\Phi_1^{(3)} + \Phi_2^{(3)}]$, which was so dominant in quasi-0D, is also dominant for the excess free energy of the solid (Fig. 9). Yet, due to the contributions of neighboring particles, the effects of the remaining relatively small contributions obtained from different trial forms (see below) for a corrected $\Phi_3^{(3)}$ are not always as expected by the quasi-0D analysis. In particular, $\Phi_{3,\text{exact-0D}}^{(3)}$ does not describe the solid more accurately than some other forms considered below. On our way towards improving the density functional theory of the hard-sphere fluid-solid transition, we still need to understand the systematics in these final steps towards the correct third term, and it is still uncertain at what level of sophistication, of the improved functional, anisotropic deviations from the Gaussian profiles [29] come in.

The result obtained from the quasi-0D analysis, namely, $\Phi_{3,\text{exact-0D}}^{(3)}$, is obviously unsuitable to describe the bulk-3D fluid, but it provides a guideline as to the appropriate modifications of the original $\Phi_3^{(3)}$ which, in turn, is accurate for quasi-3D fluids. The simplest modification of $\Phi_3^{(3)}$ which is suggested by the need to get the exact 0D limit is the ‘‘antisymmetrization.’’ In particular, we considered the following simple ‘‘antisymmetrized’’ versions of $\Phi_3^{(3)}$:

$$\Phi_{3,\text{asym}(q)}^{(3)} = \frac{\frac{1}{3}(n_2)^3}{8\pi(1-n_3)^2} (1-\xi^2)^q, \quad (27)$$

which give the same bulk-3D excess free energy as $\Phi_3^{(3)}$, and where $q \geq 2$ in order that the contribution of the term be of order Δ^2 or smaller. With $q=2$ the term is of the correct

order Δ^2 . The significance of the case $q=3$ with the form $(1-\xi^2)^3$ is that it recovers $\Phi_3^{(3)}$ by the first two terms, $1-3\xi^2$, in its ξ^2 expansion, and thus yields also the same Percus-Yevick pair direct correlations for the bulk fluid. Since the difference $[\Phi_{3,\text{asym}(3)}^{(3)} - \Phi_3^{(3)}]$ is of order ξ^4 then the functional with $\Phi_{3,\text{asym}(3)}^{(3)}$ also yields the same bulk three-particle direct correlation functions as with $\Phi_3^{(3)}$. In turn, it contributes to the quasi-0D limit the incorrect order of Δ^4 . On the other hand, the following interpolation form gives $\Phi_3^{(3)}$ in the bulk limit and is almost identical to $\Phi_{3,\text{exact-0D}}^{(3)}$ in the quasi-0D limit:

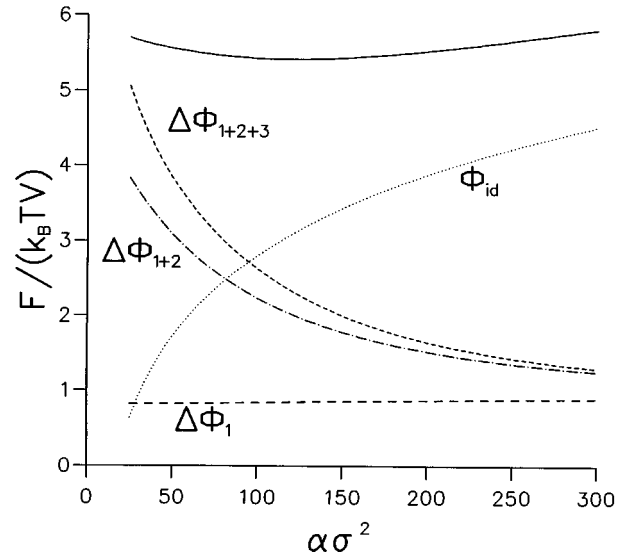


FIG. 9. Contributions of the different terms in the free-energy functional to the free-energy density $F/Vk_B T$ of the fcc hard-sphere solid as a function of the Gaussian parameter $\alpha\sigma^2$ at the melting density $\rho\sigma^3 = 6\eta/\pi = 1.0409$. The dotted line (denoted Φ_{id}) represents the ‘‘ideal’’ part of the functional, the long-dashed line ($\Delta\Phi_1$) is the contribution of the first term in the excess part of the functional, the dot-dashed line ($\Delta\Phi_{1+2}$) is that of the first and second terms, the short-dashed line ($\Delta\Phi_{1+2+3}$) is the total excess contribution using the symmetrized term $\Phi_{3,\text{asym}(3)}^{(3)}$. The solid line is the sum of the total excess and ideal contributions.

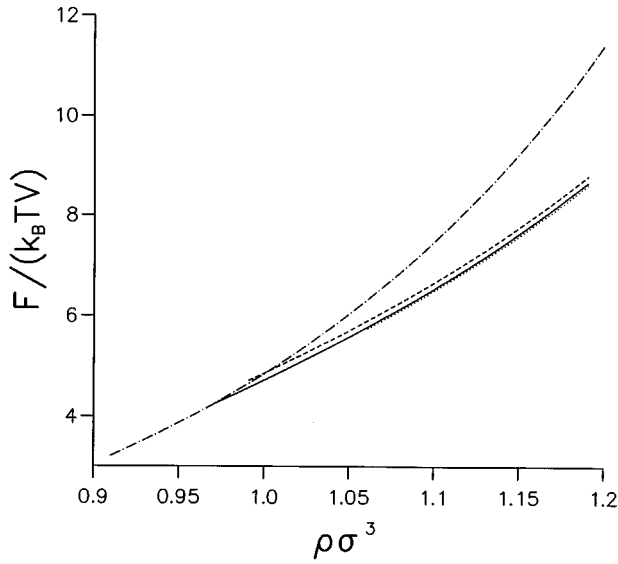


FIG. 10. Free-energy density $F/Vk_B T$ of the fcc hard-sphere solid as a function of the density $\rho\sigma^3$, as obtained with each one of the following “third” terms: $\Phi_{3,\text{asym}(3)}^{(3)}$ (solid line), $\Phi_{3,\text{asym}(2)}^{(3)}$ (dashed line), $\Phi_{3,\text{exact-0D}}^{(3)}$ (dotted line), as a function of the reduced density $\rho\sigma^3 = 6\eta/\pi$, compared with the corresponding fluid free-energy density (dash-dotted line).

$$\Phi_{3,\text{int}}^{(3)} = \frac{\frac{1}{3}(n_2)^3}{8\pi(1-n_3)^2} (1 - 3\xi^2 + 2\xi^3). \quad (28)$$

The term ξ^3 affects, however, the bulk-3D three-particle direct correlations.

As far as the properties of the solid are concerned, the four forms, $\Phi_{3,\text{exact-0D}}^{(3)}$ and $\Phi_{3,\text{asym}(q)}^{(3)}$ with $q=2$ and $q=3$, and $\Phi_{3,\text{int}}^{(3)}$, all give comparable equations of state (e.g., excess free energy and pressure) in excellent agreement with the simulations from closest packing to the melting density (Figs. 10 and 11). The results from $\Phi_{3,\text{int}}^{(3)}$ are always between those from $\Phi_{3,\text{asym}(q)}^{(3)}$ with $q=3$ and $q=2$, and are not displayed in the figures in order to make them more readable. These four forms also give comparable values for the Lindemann parameter, i.e., comparable values for the Gaussian parameter α (Fig. 12). We wish to emphasize that after obtaining the results for our initial choice [36] $\Phi_{3,\text{asym}(q)}^{(3)}$ with $q=3$, we investigated the other forms mainly in order to have a better clue to what is required for improving the values of the Gaussian widths. The fact that all these forms, and in particular $\Phi_{3,\text{exact-0D}}^{(3)}$, give about the same (and much too narrow) Gaussians is very significant. It may indicate that in order to obtain the correct Gaussian widths the correct third term of the functional must contain tensorial forms (see the discussion in the next section). Similarly much too narrow Gaussians were obtained by most previous weighted density functionals in the literature [27–29], but these functionals did not offer any way to improve the results. It should be noted that due to the dominant contribution of $[\Phi_1^{(3)} + \Phi_2^{(3)}]$, the total excess free energy as a function of α for a given density remains a very slowly varying function, so that the rather incorrect values for the Lindemann parameter (i.e., α) do not affect the quality of the equation of state.

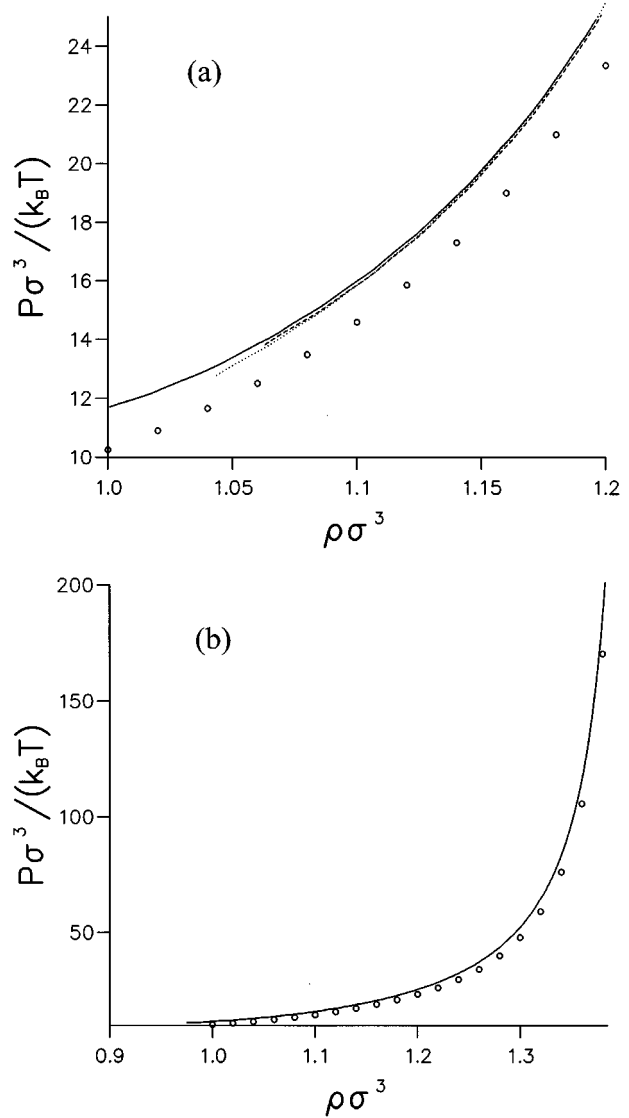


FIG. 11. (a) Pressure $P\sigma^3/k_B T$ of the fcc hard-sphere solid, as a function of the density $\rho\sigma^3$, as obtained with one of the following “third” terms: $\Phi_{3,\text{asym}(3)}^{(3)}$ (solid line), $\Phi_{3,\text{asym}(2)}^{(3)}$ (dashed line), $\Phi_{3,\text{exact-0D}}^{(3)}$ (dotted line), as a function of the reduced density $\rho\sigma^3 = 6\eta/\pi$, compared with the simulations (open circles [55]). (b) Same as (a) but for a larger density range (note that $\rho\sigma^3 = \sqrt{2}$ is the closest packing density). On this scale the dashed and dotted lines would be almost indistinguishable from the full line.

It is interesting to observe (Fig. 13) that with $\Phi_{3,\text{exact-0D}}^{(3)}$ the functional yields the solid only as a local minimum (the global minimum being a liquid, i.e., for very broad Gaussians), and that the local minimum (i.e., the solid as described above) disappears at about the correct melting density ($\eta \approx 0.54$). With $\Phi_{3,\text{int}}^{(3)}$, or with $\Phi_{3,\text{asym}(q)}^{(3)}$ (with $q=2$ or $q=3$) we obtain better solid-fluid transition parameters than almost all previous functionals in the literature when compared with simulations. In particular, for $q=3$ we get (the simulation results are given in parentheses [28,29]): the packing fraction of the fluid $\eta_F = 0.491$ (0.494), and the solid $\eta_S = 0.540$ (0.545), the melting pressure $P\sigma^3/k_B T = 12.3$ (11.7), Lindemann ratio $L = 0.101$ (0.129), and vacancy concentration $e^{-17.1}$ (≈ 0).

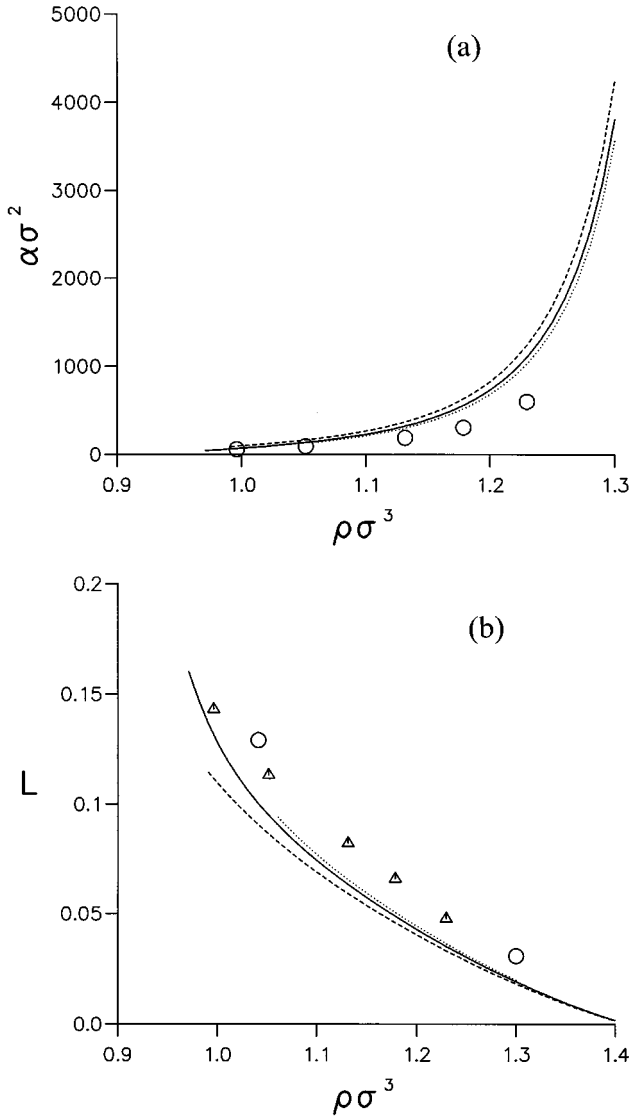


FIG. 12. (a) Gaussian parameter $\alpha\sigma^2$ of the fcc hard-sphere solid, as a function of the density $\rho\sigma^3$, as obtained with one of the following “third” terms: $\Phi_{3,\text{asym}(3)}^{(3)}$ (solid line), $\Phi_{3,\text{asym}(2)}^{(3)}$ (dashed line), $\Phi_{3,\text{exact-0D}}^{(3)}$ (dotted line), as a function of the reduced density $\rho\sigma^3 = 6\eta/\pi$, compared with the simulations (open circles [55]). (b) Same as (a) but for the Lindemann parameter $L = \sqrt{3}(\rho\sigma^3)^{1/3}/2^{2/3}\sqrt{\alpha}$, with triangles and circles representing [55,29], respectively.

The vacancy concentration $e^{-17.1}$ is obtained as follows: Let $\eta_0 \leq 1$ be the average occupancy (which corresponds to the normalization of the Gaussians). Then we have

$$\frac{\partial f}{\partial \eta_0} = \mu = \frac{\partial f}{\partial \rho} = 17.1 \quad (\text{at melting}) \quad (29)$$

but, in turn, for our functionals we have

$$\frac{\partial f}{\partial \eta_0} \approx \frac{\partial}{\partial \eta_0} f_{\text{exact-0D}}(\eta_0) = -\ln(1 - \eta_0). \quad (30)$$

This result, $1 - \eta_0 = e^{-17.1} = 3.75 \times 10^{-8}$, could be estimated from the known chemical potential of the hard-sphere solid,

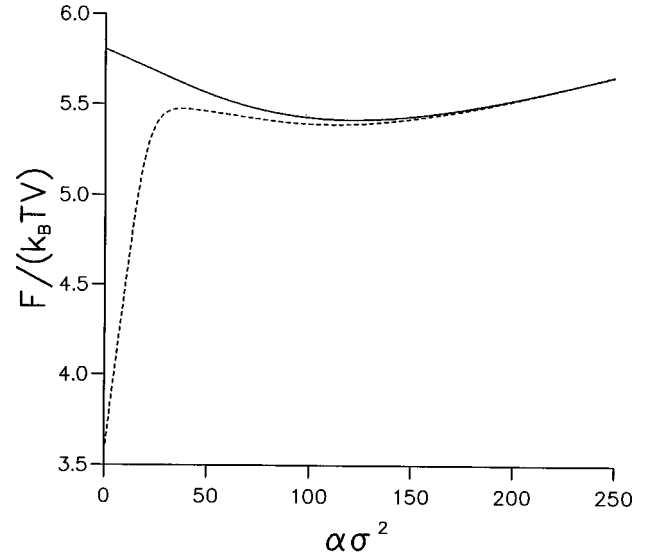


FIG. 13. The free-energy density $F/Vk_B T$ of the fcc hard-sphere solid, as obtained with $\Phi_{3,\text{asym}(3)}^{(3)}$ (solid line) and $\Phi_{3,\text{exact-0D}}^{(3)}$ (dashed line), as function of the Gaussian parameter $\alpha\sigma^2$ at the melting density $\rho\sigma^3 = 6\eta/\pi = 1.0409$.

and in practice, for numerical purposes, we have performed our calculations using $\eta_0 = 1$. If one approximates the solid by a superposition of *normalized* narrow Gaussians, then it can be stabilized by any functional that is able to achieve gross similarity with the exact result for $\eta = 1$ in the 0D limit. Due to its correct 0D properties, the fundamental-measure theory is the first that can yield the solid under completely free minimization, and the correct vacancy concentration (i.e., the normalization of the Gaussians) is obtained from the free minimization of the functional. In the application of previous functionals to freezing, it was either assumed *a priori* that $\eta_0 = 1$ [an inconsistent assumption for functionals that could not satisfy Eq. (30)], or the vacancy concentration would come out to be of order 10% or more.

None of the previous weighted density functionals in the literature featured the correct divergence of the equation of state at closest packing for the fcc lattice. Some of them showed a very steep (but finite) rise in the region of closest fcc packing: When the nearest neighbor Gaussians enter into the excluded volume sphere they have to pay a very large (but finite) free-energy price. For the bcc lattice, however, which has fewer neighbors, the rise of the pressure is much less steep [49] for these functionals, which shows that these approximations could not keep track of the individual excluded volumes. On the other hand, due to their particular building blocks, involving the geometry of the particles, the fundamental-measure functionals, e.g., with $\Phi_{3,\text{int}}^{(3)}$, $\Phi_{3,\text{asym}(q)}^{(3)}$, or $\Phi_{3,\text{exact-0D}}^{(3)}$, diverge at closest packing (CP) for any structure. Our numerical results for fcc seem to follow rather well the free-volume result, $PV/Nk_B T = [1 - (\eta/\eta_{\text{CP}})^{1/3}]^{-1}$. More recent investigation [50] reveals quite generally that fundamental-measure functionals (a) have the mechanism to locate situations of hard-sphere closest packing, (b) they can feature “symmetry breaking” that separates the solidlike and liquidlike solutions for the density profiles, and (c) they contain the free-volume cell theory as a

special limit case. Specifically, the fundamental-measure functionals that feature the exact 0D limit for a $\delta(\mathbf{x})$ distribution obey the free-volume equation of state near closest packing for any lattice structure.

VI. DISCUSSION

The fact that $\Phi_{3,\text{asym}(q)}^{(3)}$ with $q=2$ yields an almost identical solid to that obtained with $q=3$ should be considered in view of the fact that the corresponding bulk two-particle direct correlation functions $c^{(2,\text{FD})}(r)$ are significantly different. In particular, for $q=3$ $c^{(2,\text{FD})}(r)$ is the Percus-Yevick result, while for $q=2$ it contains a $1/r$ singularity at the origin. This shows that the relative importance of the details of the bulk fluid properties, for the correct description of the solid, may depend strongly on the way these are implemented in the theory. The bulk Percus-Yevick direct correlations are just one example for a convolution form obtained by the fundamental-measure functional. Different forms for the functional can be obtained with the same bulk excess free energy, different bulk direct correlations, yet with similar predictions for the solid. This ‘‘freedom’’ is one of the reasons so many different weighted density approximations in the past [28], all essentially based on the Percus-Yevick numerical input, could give reasonable solids. The fundamental-measure functionals, however, provide the bulk fluid properties as a special case, and thus enable a systematic search of the optimal functional form by imposing the correct dimensional cross-over and freezing properties as physical constraints on the functional form of the excess free energy.

The $1/r$ singularity in the pair direct correlation obtained from the functional Eq. (13), as we noticed in the 2D limit, exists for arbitrarily small nonuniformity of the 3D density profile, $\Delta\rho(\mathbf{r}) = \rho(\mathbf{r}) - \rho_0$, for which the vector densities are nonzero. This singularity does not contribute to the pair direct correlations in the bulk-3D limit, where the vector weighted densities \mathbf{n}_2 vanish. Since the nonuniform pair direct correlation function can be expanded around its $\rho(\mathbf{r}) = \rho_0$ uniform fluid limit, in powers of $\Delta\rho(\mathbf{r})$, then the 3D bulk three-particle direct correlation function must also contain singular terms (Appendix B). Recall, however, that the 3D bulk three-particle direct correlation function, as obtained from the same 3D functional, was calculated in k space [31,42,43] and was found to agree well with the simulation data, so that the singularity apparently does not affect much the resulting Fourier transforms. In general, the convolution of two δ functions in $D=3$ leads to a $1/r$ -type singularity, which is thus inherent to the geometric description. In turn we found out that the geometric weight functions are essential for obtaining the correct 0D limit. Thus all singularities must eventually be canceled out by a correct functional form for $\Phi^{(D)}[\{n_\alpha(\mathbf{x})\}]$. Even though the cancellation is incomplete for Eq. (13), it does not affect the high accuracy of the density profiles [30–35, 42–44] as obtained from it for a large variety of confinement situations. Moreover, in most situations we can just ignore the singular terms in the pair direct correlations of the inhomogeneous fluid, corresponding to minor changes in $\Phi^{(D=3)}$ for a small free-energy price.

The exact 3D functional for hard spheres will contain au-

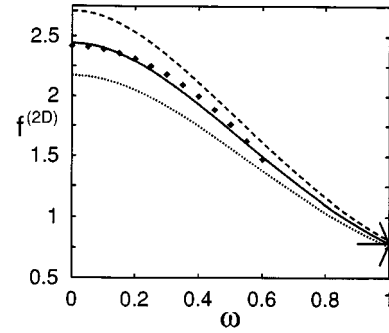


FIG. 14. Same as Fig. 4 but using the new third term $\Phi_{3,\text{asym}(3)}^{(3)}$, for several values of λ (from top $\lambda = 1, 0.5, 0$).

tomatically all the required ‘‘mechanisms’’ to make it obey the 2D, 1D, and 0D limits. Our task was to identify these mechanisms within the class of functionals which are constructed through the fundamental geometric measures of the particles. These functionals feature the exact 1D functional when applied directly to hard rods, and yield a unified scaled-particle Percus-Yevick theory when applied to 3D spheres. We have demonstrated that the 3D functional, when taken in the 0D, 1D, and 2D limits, can reproduce basic properties of the 0D, 1D, and 2D functionals, respectively. We have found that by enlarging a little the simplest basis set $\{\varphi_I\}$ we can significantly improve the crossover properties of the simplest functional Eq. (13).

As part of the subtle interplay of the dimensional cross-over, the antisymmetrized form, which is suggested by the need to get the exact 0D limit, also affects the *bridge* functional near the bulk-3D limit [51]. With $\Phi_{3,\text{asym}(3)}^{(3)}$ the initial slope of the nonadditive hard-disk limit of the functional is negative as it should physically be (Appendix B and Fig. 14). The contribution of the new $\Phi_{3,\text{asym}(3)}^{(3)}$ does not strictly vanish in the bulk quasi-1D limit, as required to give the exact result, but it is generally very small, except near $\eta=1$ where it dominates (Appendix C and Fig. 15). In the quasi-2D limit it performs about as well as $\Phi_3^{(3)}$ (Appendix A and Fig. 16), but the $1/r$ singularity is of opposite sign (Fig. 17). Our functional provided very accurate density profiles when compared with simulations for hard spheres confined between

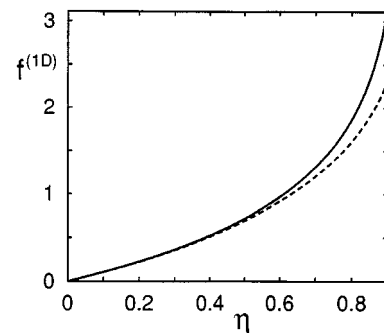


FIG. 15. Excess free energy for hard rods, $f_{\text{ex}}^{(1D)}$, as a function of the packing fraction η , as obtained from the first two terms of the functional, Eq. (C9), i.e., the exact 1D result (dashed line), compared with that obtained by adding the contribution of $\Phi_{3,\text{asym}(3)}^{(3)}$ [see Eq. (C18)], solid line.

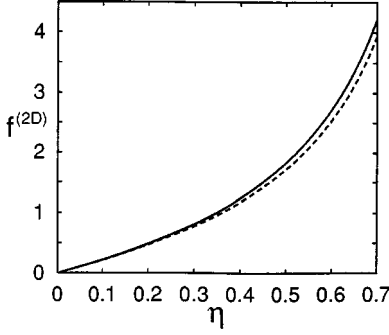


FIG. 16. Excess free energy for hard disks, $f_{\text{ex}}^{(2D)}$, as a function of the packing fraction η , as obtained with $\lambda=1$ in Eq. (A14), dashed line, compared with that obtained by replacing $\Phi_3^{(3)}$ with $\Phi_{3,\text{asym}(3)}$ [see Eq. (A39)], solid line.

very narrow plates (quasi-2D situations) [52].

The fundamental-measure weighted densities were found to have many correct properties, but they cannot be expected to provide the complete basis set for the exact functional. Yet, as we have demonstrated, our approach enables systematic analysis and systematic improvement of the approximate fundamental-measure functional. In view of their role in the 1D and 0D limits, the first two terms, $\Phi_1^{(3)}$ and $\Phi_2^{(3)}$, seem to be correct. More insight is needed in order to reach the optimal third term $\Phi_3^{(3)}$. The desirable $\Phi_3^{(3)}$ should ultimately have also the following properties: (i) cancel out the $1/r$ singularity, (ii) should not contribute in the 1D limit, (iii) behave like $\Phi_{3,\text{exact-0D}}^{(3)}$ in the quasi-0D limit, (iv) behave like $\approx \frac{1}{2}\Phi_3^{(3)}$, of Eq. (13), in the 2D limit, and (v) give the correct Lindemann parameter of the solid. These desirable properties are probably interrelated, and we have indications that some of them, if not all, can be achieved by replacing the factor $(1-\xi^2)^q$ in Eq. (27) with slightly more complicated forms, including tensorial terms like $\sum M_{ijk}\xi_i\xi_j\xi_k$, involving the elements of the dimensionless vector $\hat{\xi} \equiv \mathbf{n}_{V2}/n_2 = (\xi_x, \xi_y, \xi_z)$. The analysis of the fundamental-measure theory as applied to parallel hard cubes [53] may prove useful. We demonstrated the special role played by the fundamental-measure functional, as derived from ‘‘liquid’’ considerations and adjusted to the exact 0D limit, for obtaining the correct descrip-

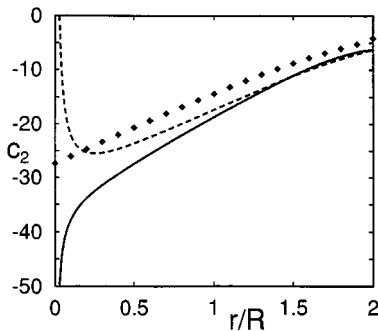


FIG. 17. Direct correlation function $c^{(2,\text{FD})}(r)$, for the hard disks at $\eta=0.6$. The diamonds give the solution of the Percus-Yevick equation [47]. The dashed line obtained by using $\Phi_3^{(3)}$ (compare with Fig. 5), and the solid line by using $\Phi_{3,\text{asym}(3)}$. Note the opposite sign of the $1/r$ behavior near the origin.

tion of the solid. Its understanding may lead to a better understanding of the density functional theory of freezing. Pending further progress along these lines, the new third term $\Phi_{3,\text{asym}(3)}$ [which in the notations of Eq. (16) corresponds to the prefactor $\lambda = (1-\xi^2)^3/1-3\xi^2$] already provides a free-energy functional for 3D hard-sphere fluids with adequate properties of dimensional crossover.

ACKNOWLEDGMENTS

H.L., Y.R., and M.S. thank Professor Herbert Wagner for interesting discussions, warm hospitality, and generous support at the Ludwig Maximilians Universität München. Y.R. thanks Professor Bob Evans for many enlightening discussions, his warm hospitality at Bristol University, and for his many kindnesses that enabled an exciting itinerant sabbatical in Europe. The warm and stimulating hospitality of Professor David Gonzalez and Dr. Luis Gonzalez in Valladolid, and of Professor Jean-Pierre Hansen and Dr. Thierry Biben in Lyon (where the present paper was completed) are acknowledged with gratitude. This work was supported by the Benjamin Meaker Foundation at Bristol University, the Deutsche Forschungsgemeinschaft (Gerhard Hess Program), Grant No. SAB95-0340 from the Spanish Ministry of Science and Education, and the Nicolas Cabrera Institute in Madrid.

APPENDIX A: EXCESS FREE ENERGY AND PAIR DIRECT CORRELATION FUNCTIONS IN THE 2D LIMIT OF THE 3D FUNCTIONAL

For a one-component hard-sphere system in slab geometry

$$\rho(\mathbf{r}) = \rho(z) \quad (\text{A1})$$

the fundamental-measure excess free-energy functional takes the form

$$\frac{\beta F_{\text{ex}}[\{\rho(\mathbf{r})\}; \lambda]}{A} = \int dz \Phi(z, \lambda) \equiv \int dz \Phi[\{n_\alpha(z)\}, \lambda], \quad (\text{A2})$$

where the weighted densities $n_\alpha(\mathbf{x}) = n_\alpha(z)$ are given by [34,43]

$$n_3(z) = \pi \int_{z-R}^{z+R} \rho(z') [R^2 - (z' - z)^2] dz', \quad (\text{A3})$$

$$n_2(z) = 2\pi R \int_{z-R}^{z+R} \rho(z') dz', \quad (\text{A4})$$

$$\mathbf{n}_{V2}(z) = \left(-2\pi \int_{z-R}^{z+R} \rho(z') (z' - z) dz' \right) \hat{\mathbf{z}} \equiv n_{V2}(z) \hat{\mathbf{z}}, \quad (\text{A5})$$

$$n_0(z) = \frac{n_2(z)}{4\pi R^2}, \quad n_1(z) = \frac{n_2(z)}{4\pi R}, \quad \mathbf{n}_{V1}(z) = \frac{\mathbf{n}_{V2}(z)}{4\pi R}. \quad (\text{A6})$$

In the 2D limit

$$\rho(z) = \rho^{(2D)} \delta(z), \quad (\text{A7})$$

where $\rho^{(2D)} = N/A =$ number of spheres divided by the area of the slab, i.e., the 2D density, these weighted densities take the form

$$n_3(z) = \pi \rho^{(2D)} (R^2 - z^2) \Theta(R - |z|), \quad (\text{A8})$$

$$n_2(z) = 2 \pi \rho^{(2D)} R \Theta(R - |z|), \quad (\text{A9})$$

$$\mathbf{n}_{V2}(z) = (2 \pi \rho^{(2D)} z) \Theta(R - |z|) \hat{\mathbf{z}}, \quad (\text{A10})$$

where $\Theta(x) = 1$ for $x \geq 0$ and $\Theta(x) = 0$ for $x < 0$. The 2D packing fraction is defined by $\eta = \rho^{(2D)} \pi R^2$. Measuring length in units R , and letting $R = 1$, then the weighted densities are given by

$$n_3(z) = \eta (1 - z^2) \Theta(1 - |z|), \quad (\text{A11})$$

$$n_2(z) = 2 \eta \Theta(1 - |z|), \quad n_1(z) = \frac{\eta}{2\pi} \Theta(1 - |z|),$$

$$n_0(z) = \frac{\eta}{2\pi} \Theta(1 - |z|), \quad (\text{A12})$$

$$\mathbf{n}_{V2}(z) = (2 \eta z) \Theta(1 - |z|) \hat{\mathbf{z}},$$

$$\mathbf{n}_{V1}(z) = \left(\frac{\eta}{2\pi} z \right) \Theta(1 - |z|) \hat{\mathbf{z}}. \quad (\text{A13})$$

The excess free energy per particle can be obtained analytically [34,43]:

$$\begin{aligned} f^{(2D)}(\lambda, \eta) &= \frac{(1/k_B T) F_{\text{ex}}[\{\rho(\mathbf{r})\}]}{N} = \int_{-1}^1 dz \Phi(z) / \rho^{(2D)} \\ &= \lambda \eta + \frac{\lambda \eta^2}{3(1-\eta)} + \left(2 - \lambda + \frac{\lambda \eta}{3(1-\eta)} \right) \\ &\quad \times \sqrt{\frac{\eta}{1-\eta}} \arctan \left(\sqrt{\frac{\eta}{1-\eta}} \right) \end{aligned} \quad (\text{A14})$$

and this result agrees with the previous results [34,43] for $\lambda = 1$.

The direct correlation function coefficients $\Psi_{\alpha\beta} = \Phi''_{\alpha\beta} = \partial^2 \Phi / \partial n_\alpha \partial n_\beta$ for the functional (13), i.e., using $\Phi_3^{(3)}$, are given by

$$\Psi_{03} = \Psi_{30} = \Psi_{12} = \Psi_{21} = \frac{1}{1-n_3}, \quad (\text{A15})$$

$$\Psi_{V1V2} = \Psi_{V2V1} = -\frac{1}{1-n_3}, \quad (\text{A16})$$

$$-\Psi_{22} = \Psi_{V2V2} = -\lambda \frac{n_2}{4\pi(1-n_3)^2}, \quad (\text{A17})$$

$$\Psi_{13} = \Psi_{31} = \frac{n_2}{(1-n_3)^2}, \quad (\text{A18})$$

$$\Psi_{23} = \Psi_{32} = \frac{n_1}{(1-n_3)^2} + \lambda \frac{n_2^2 - \mathbf{n}_{V2} \cdot \mathbf{n}_{V2}}{4\pi(1-n_3)^3}, \quad (\text{A19})$$

$$\begin{aligned} \Psi_{33} &= \frac{n_0}{(1-n_3)^2} + \frac{2n_1 n_2 - 2\mathbf{n}_{V1} \cdot \mathbf{n}_{V2}}{(1-n_3)^3} \\ &\quad + \lambda \frac{n_2^3 - 3n_2 \mathbf{n}_{V2} \cdot \mathbf{n}_{V2}}{4\pi(1-n_3)^4}, \end{aligned} \quad (\text{A20})$$

$$\Psi_{3,V1} = \Psi_{V1,3} = -\frac{\mathbf{n}_{V2}}{(1-n_3)^2}, \quad (\text{A21})$$

$$\Psi_{3,V2} = \Psi_{V2,3} = -\frac{\mathbf{n}_{V1}}{(1-n_3)^2} - \lambda \frac{n_2 \mathbf{n}_{V2}}{2\pi(1-n_3)^3}, \quad (\text{A22})$$

$$\Psi_{2,V2} = \Psi_{V2,2} = -\lambda \frac{\mathbf{n}_{V2}}{4\pi(1-n_3)^2}. \quad (\text{A23})$$

The two-particle direct correlation function for a pair at distance r in the plane $z = 0$, parallel to the slab walls [r is in units of $R = 1$, and recall that $c(r > 2R) = 0$] is written in the form

$$-c(r, \lambda) = -c_U(r, \lambda) - c_N(r, \lambda), \quad (\text{A24})$$

where

$$\begin{aligned} -c_U(r, \lambda) &= \int_{-z_{\text{max}}(r)}^{z_{\text{max}}(r)} \Psi_{33}(z, \lambda) f_V(z, r) dz \\ &\quad + \int_{-z_{\text{max}}(r)}^{z_{\text{max}}(r)} \Psi_{23}(z, \lambda) f_S(z, r) dz \\ &\quad + \int_{-z_{\text{max}}(r)}^{z_{\text{max}}(r)} \left[\Psi_{13}(z) \frac{f_S(z, r)}{4\pi} \right. \\ &\quad \left. + [\Psi_{22}(z, \lambda) + \theta(r) \Psi_{V2,V2}(z, \lambda)] 2g(z, r) \right] dz \\ &\quad + \int_{-z_{\text{max}}(r)}^{z_{\text{max}}(r)} \left[\Psi_{03}(z) \frac{f_S(z, r)}{4\pi} \right. \\ &\quad \left. + [\Psi_{12}(z, \lambda) + \theta(r) \Psi_{V1,V2}(z, \lambda)] \frac{g(z, r)}{\pi} \right] dz \end{aligned} \quad (\text{A25})$$

contains the terms that contribute to the uniform (bulk) 3D fluid result, and

$$\begin{aligned} -c_N(r, \lambda) &= \int_{-z_{\text{max}}(r)}^{z_{\text{max}}(r)} \xi_{V1,3}(z) \frac{|z|}{4\pi} f_S(z, r) dz \\ &\quad + \int_{-z_{\text{max}}(r)}^{z_{\text{max}}(r)} \xi_{V2,3}(z, \lambda) |z| f_S(z, r) dz \\ &\quad + \int_{-z_{\text{max}}(r)}^{z_{\text{max}}(r)} \xi_{V2,2}(z, \lambda) 4|z| g(z, r) dz \end{aligned} \quad (\text{A26})$$

contains the remaining terms (which may contribute in the general nonuniform fluid case). We defined

$$\Psi_{V1,3} = \xi_{V1,3} \hat{\mathbf{z}}, \quad \Psi_{V2,3} = \xi_{V2,3} \hat{\mathbf{z}}, \quad \Psi_{2,V2} = \xi_{2,V2} \hat{\mathbf{z}}, \quad (\text{A27})$$

$$z_{\max}(r) = \sqrt{1 - \left(\frac{r}{2}\right)^2}, \quad Y = \sqrt{1 - z^2}, \quad \theta(r) = 1 - \frac{r^2}{2}, \quad (\text{A28})$$

$$\int_{-z_{\max}(r)}^{z_{\max}(r)} \left[\frac{f_S(z, r)}{4\pi} + \frac{1}{2\pi} [1 - \theta(r)] g(z, r) \right] dz = \Delta R(r), \quad (\text{A34})$$

$$f_V(z, r) = Y^2 \left\{ \pi - 2 \sqrt{1 - \left(\frac{r}{2Y}\right)^2} \left(\frac{r}{2Y}\right) - 2 \arcsin\left(\frac{r}{2Y}\right) \right\}, \quad (\text{A29})$$

$$\int_{-z_{\max}(r)}^{z_{\max}(r)} \left[\frac{f_S(z, r)}{4\pi} + \frac{1}{\pi} [1 - \theta(r)] g(z, r) \right] dz = \Theta(2 - r), \quad (\text{A35})$$

and thus also

$$f_S(z, r) = 4 \arccos\left(\frac{r}{2Y}\right), \quad \Delta R(r \leq 2) = \frac{1}{2} \left(1 + \frac{\Delta S(r)}{4\pi} \right). \quad (\text{A36})$$

$$g(z, r) = \frac{1}{r \sqrt{1 - (r/2)^2 - z^2}}. \quad (\text{A30})$$

In order to check the geometric factors in these expressions, we considered also the uniform fluid limit (with $\lambda = 1$) where by comparison with [31,39] we verified that.

$$\int_{-z_{\max}(r)}^{z_{\max}(r)} f_V(z, r) dz = \Delta V(r) = \frac{4\pi}{3} \left[1 - \frac{3}{2}(r/2) + \frac{1}{2}(r/2)^3 \right], \quad (\text{A31})$$

$$\int_{-z_{\max}(r)}^{z_{\max}(r)} f_S(z, r) dz = \Delta S(r) = 4\pi [1 - (r/2)], \quad (\text{A32})$$

$$\int_{-z_{\max}(r)}^{z_{\max}(r)} \left[\frac{1}{2\pi} [1 - \theta(r)] g(z, r) \right] dz = \frac{1}{2}(r/2), \quad (\text{A33})$$

The function associated with the convolutions of two δ functions, $g(z, r)$, contains a $1/r$ singularity which is canceled by the factor $[1 - \theta(r)]$ in the terms that contribute to pair direct correlation functions of the uniform 3D fluid, c_U , i.e., the singularity as appears in the convolution of scalar-surface characteristic functions cancels out by that from the vector functions. This cancellation does not work in c_N . The reason this singularity does not show up in the uniform 3D limit is because the vector weighted densities vanish in that limit, i.e., the functions (A21)–(A23) vanish in that limit, making $c_N = 0$.

The singularity found above for the 2D limit exists for arbitrarily small nonuniformity of the density profile which will make the vector densities nonzero, and as a result, the noncanceled singularity from the convolution of surface characteristic functions will contribute. The nonuniform pair direct correlation function can be expanded around its uniform fluid limit, $\rho_i(\mathbf{r}) = \rho_i^{(0)}$, in powers of the deviations of the density profiles from uniformity, $\Delta \rho_i(\mathbf{r}) = \rho_i(\mathbf{r}) - \rho_i^{(0)}$,

$$c_{i_1, i_2}^{(2, \text{FD})}(\mathbf{r}_1, \mathbf{r}_2) = c_{i_1, i_2}^{(2, \text{FD}), (0)}(r = |\mathbf{r}_1 - \mathbf{r}_2|) + \sum_{i_3} \int c_{i_1, i_2, i_3}^{(3, \text{FD}), (0)}(|\mathbf{r}_1 - \mathbf{r}_3|, |\mathbf{r}_2 - \mathbf{r}_3|) \Delta \rho_{i_3}(\mathbf{r}_3) d\mathbf{r}_3 + \dots, \quad (\text{A37})$$

which, for the functional (13), takes the form

$$\begin{aligned} c_{i_1, i_2}^{(2, \text{FD})}(\mathbf{r}_1, \mathbf{r}_2) &= - \int d\mathbf{x} \sum_{\alpha, \beta} \Psi_{\alpha\beta}[\{n_\gamma(\mathbf{x})\}] w_{i_1}^{(\alpha)}(\mathbf{x} - \mathbf{r}_1) w_{i_2}^{(\beta)}(\mathbf{x} - \mathbf{r}_2) \\ &= - \int d\mathbf{x} \sum_{\alpha, \beta} \Psi_{\alpha\beta}[\{n_\gamma^{(0)}\}] w_{i_1}^{(\alpha)}(\mathbf{x} - \mathbf{r}_1) w_{i_2}^{(\beta)}(\mathbf{x} - \mathbf{r}_2) - \sum_{i_3} \int \left[\int d\mathbf{x} \sum_{\alpha, \beta, \gamma} \Psi_{\alpha\beta\gamma}[\{n_\gamma^{(0)}\}] w_{i_1}^{(\alpha)}(\mathbf{x} - \mathbf{r}_1) \right. \\ &\quad \left. \times w_{i_2}^{(\beta)}(\mathbf{x} - \mathbf{r}_2) w_{i_3}^{(\gamma)}(\mathbf{x} - \mathbf{r}_3) \right] \Delta \rho_{i_3}(\mathbf{r}_3) d\mathbf{r}_3 + \dots \end{aligned} \quad (\text{A38})$$

Thus if $c_{i_1, i_2}^{(2, \text{FD})}(\mathbf{r}_1, \mathbf{r}_2)$ contains a singularity then the 3D bulk three-particle direct correlation function $c_{i_1, i_2, i_3}^{(3, \text{FD}), (0)}(|\mathbf{r}_1 - \mathbf{r}_3|, |\mathbf{r}_2 - \mathbf{r}_3|)$ must contain singular terms. In particular, in the pairs of terms associated with the coefficients $\Psi_{\alpha\beta\gamma} = \Psi_{2,2,2}$ and $\Psi_{V2,V2,2}$, as well as in those associated with $\Psi_{\alpha\beta\gamma} = \Psi_{1,2,3}$ and $\Psi_{V1,V2,3}$, and $\Psi_{\alpha\beta\gamma} = \Psi_{2,1,3}$

and $\Psi_{V2,V1,3}$, the singularity cancels out. The singularity does remain, however, in the terms associated with $\Psi_{\alpha\beta\gamma} = \Psi_{2,V2,V2}$ and $\Psi_{V2,2,V2}$.

The change in the bulk-2D limit of the excess free energy resulting from replacing the original $\Phi_3^{(3)}$ with the new third term, $\Phi_{3, \text{asym}}^{(3)}$, is given by

$$\begin{aligned}\Delta f^{(2D)}(\eta) &= \int_{-1}^1 dz [\Phi_{3,\text{asym}(3)}^{(3)}(z) - \Phi_3^{(3)}(z)] / \rho^{(2D)} \\ &= \eta^2 \int_{-1}^1 \left[\frac{z^4 - z^6/3}{[1 - \eta(1 - z^2)]^2} \right] dz. \quad (\text{A39})\end{aligned}$$

The ratio $\Delta f^{(2D)}(\eta)/f^{(2D)}(1, \eta)$ is an increasing function of η which is very small and reaches a value of only about 0.06 at $\eta=0.8$ (see Fig. 16).

When we replace $\Phi_3^{(3)}$ by the new symmetrized form $\Phi_{3,\text{sym}(3)}^{(3)}$, the direct correlation function coefficients $\Psi_{\alpha\beta} = \Phi_{\alpha\beta}''$ which change are the following (see the text):

$$\Psi_{22} = \lambda \frac{n_2}{4\pi(1-n_3)^2} (1 + \xi^4 - 2\xi^6), \quad (\text{A40})$$

$$\Psi_{v_2v_2} = -\lambda \frac{n_2}{4\pi(1-n_3)^2} (1 - 6\xi^2 + 5\xi^4), \quad (\text{A41})$$

$$\Psi_{2,v_2} = \lambda \frac{\mathbf{n}_{v_2}}{4\pi(1-n_3)^2} (1 + 2\xi^2 - 3\xi^4), \quad (\text{A42})$$

$$\Psi_{3,v_2} = -\frac{\mathbf{n}_{v_1}}{(1-n_3)^2} - \lambda \frac{n_2 \mathbf{n}_{v_2}}{2\pi(1-n_3)^3} (1 - \xi^2)^2, \quad (\text{A43})$$

$$\Psi_{23} = \Psi_{32} = \frac{n_1}{(1-n_3)^2} + \lambda \frac{n_2^2}{4\pi(1-n_3)^3} (1 - \xi^2)^2 (1 + \xi^2), \quad (\text{A44})$$

$$\begin{aligned}\Psi_{33} &= \frac{n_0}{(1-n_3)^2} + \frac{2n_1n_2 - 2\mathbf{n}_{v_1} \cdot \mathbf{n}_{v_2}}{(1-n_3)^3} \\ &+ \lambda \frac{n_2^3}{4\pi(1-n_3)^4} (1 - \xi^2)^3. \quad (\text{A45})\end{aligned}$$

APPENDIX B: EXCESS FREE ENERGY OF NONADDITIVE HARD DISKS AS A 2D LIMIT OF THE 3D FUNCTIONAL

Following Ref. [43], consider a binary mixture of hard spheres with radii R_1 and R_2 in the 2D limit with densities

$$\rho_1(z) = \rho_1^{(2D)} \delta(z + \omega), \quad \rho_2(z) = \rho_2^{(2D)} \delta(z - \omega), \quad (\text{B1})$$

where $\rho_1^{(2D)} = N_1/A$, $\rho_2^{(2D)} = N_2/A$ are the numbers of spheres divided by the area of the slab, i.e., the 2D densities. This system is equivalent to a mixture of nonadditive hard disks with $R_{12} = \frac{1}{2}[(R_1 + R_2)^2 - (2\omega)^2]^{1/2}$. For small values of ω the *negative* nonadditivity parameter is $\Delta \equiv [2R_{12} - (R_1 + R_2)]/(R_1 + R_2) = -\omega^2/\frac{1}{2}(R_1 + R_2)^2$. The weighted densities take the form

$$\begin{aligned}n_3(z) &= \pi \rho_1^{(2D)} (R_1^2 - (z + \omega)^2) \Theta(R_1 - |(z + \omega)|) \\ &+ \pi \rho_2^{(2D)} (R_2^2 - (z - \omega)^2) \Theta(R_2 - |(z - \omega)|),\end{aligned} \quad (\text{B2})$$

$$\begin{aligned}n_2(z) &= 2\pi \rho_1^{(2D)} R_1 \Theta(R_1 - |z + \omega|) \\ &+ 2\pi \rho_2^{(2D)} R_2 \Theta(R_2 - |z - \omega|),\end{aligned} \quad (\text{B3})$$

$$\begin{aligned}\mathbf{n}_{v_2}(z) &= [2\pi \rho_1^{(2D)}(z + \omega)] \Theta(R_1 - |z + \omega|) \hat{\mathbf{z}} \\ &+ [2\pi \rho_2^{(2D)}(z - \omega)] \Theta(R_2 - |z - \omega|) \hat{\mathbf{z}},\end{aligned} \quad (\text{B4})$$

where $\Theta(x) = 1$ for $x \geq 0$ and $\Theta(x) = 0$ for $x < 0$. The integral

$$\frac{(1/k_B T) F_{\text{ex}}[\{\rho(\mathbf{r})\}]}{A} = \int_{-R_1 - \omega}^{R_2 + \omega} dz \Phi(z) \quad (\text{B5})$$

can be calculated analytically, but the expressions are lengthy. In order to demonstrate our point we focus attention on the simplest case when $R_1 = R_2 = R = 1$, $\rho_1^{(2D)} = \rho_2^{(2D)}$, so that $2\pi \rho_1^{(2D)} = 2\pi \rho_2^{(2D)} = \eta$, $\rho^{(2D)} = \rho_1^{(2D)} + \rho_2^{(2D)} = \eta/\pi$, and $\Delta = -\omega^2$. We noticed that by defining

$$\begin{aligned}w(\lambda, \eta, \omega^2, z^2) &= -\frac{\eta}{2\pi} \ln(1 - \eta + \eta\omega^2 + \eta z^2) \\ &+ \frac{\eta^2}{\pi} \frac{(1 - z^2)}{(1 - \eta + \eta\omega^2 + \eta z^2)} \\ &+ \lambda \frac{\eta^3}{\pi} \frac{(\frac{1}{3} - z^2)}{(1 - \eta + \eta\omega^2 + \eta z^2)^2}\end{aligned} \quad (\text{B6})$$

we can calculate the free energy in the following form:

$$\begin{aligned}f^{(2D)}(\lambda, \eta, \omega) &= \frac{(1/k_B T) F_{\text{ex}}[\{\rho(\mathbf{r})\}]}{N} \\ &= \frac{1}{(\eta/\pi)} \int_{-1-\omega}^{1+\omega} dz \Phi(z) \\ &= \frac{2}{(\eta/\pi)} \left(\int_0^{1-\omega} w(\lambda, \eta, \omega^2, z^2) dz \right. \\ &\quad \left. + \int_{1-2\omega}^1 w(\lambda, \eta/2, 0, z^2) dz \right). \quad (\text{B7})\end{aligned}$$

We checked that $f^{(2D)}(\lambda, \eta, 0) = f^{(2D)}(\lambda, \eta)$ as defined in Appendix C below. We also check that $f^{(2D)}(\lambda, \eta, \omega = 1) = f^{(2D)}(\lambda, \eta/2, \omega = 0)$, which is a general result that follows by construction and from the weight functions having the range of the particles. This relation should be compared with the exact result [45] $f_{\text{exact}}^{(2D)}(\eta, \Delta = -1) = f_{\text{exact}}^{(2D)}(\eta/2, \Delta = 0)$.

The function $f^{(2D)}(\lambda, \eta, \omega)$ has the following expansion in powers of ω :

$$\begin{aligned}f^{(2D)}(\lambda, \eta, \omega) &= f^{(2D)}(\lambda, \eta) + a_1(\lambda, \eta) \omega \\ &+ a_2(\lambda, \eta) [-\omega^2] + \dots,\end{aligned} \quad (\text{B8})$$

where

$$\begin{aligned}
a_1(\lambda, \eta) &= \left[\frac{\partial f^{(2D)}(\lambda, \eta, \omega)}{\partial \omega} \right]_{\omega=0} \\
&= \frac{2}{(\eta/\pi)} [-w(\lambda, \eta, 0, 1) + 2w(\lambda, \eta/2, 0, 1)] = \lambda \eta^2
\end{aligned} \tag{B9}$$

vanishes for $\lambda=0$, and where

$$\begin{aligned}
a_2(\lambda=0, \eta) &= -\frac{1}{2} \left[\frac{\partial^2 f^{(2D)}(\lambda=0, \eta, \omega)}{\partial \omega^2} \right]_{\omega=0} \\
&= \left(\frac{\eta}{1-\eta} \right) \left\{ 1 + \sqrt{\frac{\eta}{1-\eta}} \right. \\
&\quad \left. \times \left[\arctan \sqrt{\left(\frac{\eta}{1-\eta} \right)} \right] \right\}.
\end{aligned} \tag{B10}$$

Given the nonadditivity parameter Δ , the exact excess free energy for the 2D hard-disk fluid is expected to have the expansion [45]

$$f_{\text{exact}}^{(2D)}(\eta, \Delta) = f_{\text{exact}}^{(2D)}(\eta) + a_{2,\text{exact}}^{(2D)}(\eta)\Delta + \dots \tag{B11}$$

where

$$a_{2,\text{exact}}^{(2D)}(\eta) \cong \eta \frac{\partial f_{\text{exact}}^{(2D)}(\eta)}{\partial \eta}. \tag{B12}$$

The exact 2D result is well approximated [54] by the scaled-particle result

$$f_{\text{exact}}^{(2D)}(\eta) \cong f_{\text{SPT}}^{(2D)}(\eta) = \frac{\eta}{1-\eta} - \ln(1-\eta) \tag{B13}$$

and

$$\eta \frac{\partial f_{\text{SPT}}^{(2D)}(\eta)}{\partial \eta} = \eta \frac{2-\eta}{(1-\eta)^2} \tag{B14}$$

compares well (especially with $\lambda \cong 0.5$) with

$$\begin{aligned}
&\eta \frac{\partial f^{(2D)}(\lambda, \eta, \omega=0)}{\partial \eta} \\
&= \frac{1}{(1-\eta)^2} \left\{ \eta \left[1 - \eta + \lambda \left(\frac{1}{2} + \frac{2\eta(\eta-1)}{3} \right) \right] \right. \\
&\quad \left. + \left[1 - \eta + \lambda \left(\eta - \frac{1}{2} \right) \right] \sqrt{\frac{\eta}{1-\eta}} \left(\arctan \sqrt{\frac{\eta}{1-\eta}} \right) \right\}.
\end{aligned} \tag{B15}$$

Moreover, it compares reasonably also with $a_2(\lambda=0, \eta)$. Recall, however, that $\Delta = -\omega^2$, and thus the correct expansion type [i.e., without the $a_1(\lambda, \eta)\omega$ term], is achieved only with $\lambda=0$. For $\lambda>0$ we have $f^{(2D)}(\lambda, \eta, \omega) > f^{(2D)}(\lambda, \eta)$ for

small values of ω , which is unphysical. Yet, for $\Delta < \sim 0.1$ we find numerically that $f^{(2D)}(\lambda, \eta, \omega)$, especially with $\lambda \cong 0.5$, agrees well with the expansion of $f_{\text{exact}}^{(2D)}(\eta, \Delta)$ as approximated by the scaled-particle theory, and with $f_{\text{exact}}^{(2D)}(\eta, \Delta = -1)$.

For the new third term, $\Phi_{3,\text{asym}}^{(3)}$, the same analysis as above can be repeated using

$$\begin{aligned}
w(\lambda, \eta, \omega^2, z^2) &= -\frac{\eta}{2\pi} \ln(1 - \eta + \eta\omega^2 + \eta z^2) \\
&\quad + \frac{\eta^2}{\pi} \frac{(1-z^2)}{(1-\eta + \eta\omega^2 + \eta z^2)} \\
&\quad + \lambda \frac{\eta^3}{\pi} \frac{\frac{1}{3}(1-z^2)^3}{(1-\eta + \eta\omega^2 + \eta z^2)^2}.
\end{aligned} \tag{B16}$$

The results using this term are numerically similar to those using the original $\Phi_3^{(3)}$, except that the unphysical linear term now vanishes, $a_1(\lambda, \eta) = 0$.

APPENDIX C: EXCESS FREE ENERGY AND PAIR DIRECT CORRELATION FUNCTIONS IN THE 1D LIMIT OF THE 3D FUNCTIONAL

In the 1D limit

$$\rho(x, y) = \rho^{(1D)} \delta(x) \delta(y), \tag{C1}$$

where $\rho^{(1D)} = NeL$ is the number of spheres divided by the length of the line, i.e., the 1D density, we let t denote the radial coordinate in the plane perpendicular to the line,

$$t = \sqrt{x^2 + y^2}, \quad \hat{\mathbf{t}} = \frac{x\hat{\mathbf{x}} + y\hat{\mathbf{y}}}{\sqrt{x^2 + y^2}} \tag{C2}$$

and the weighted densities take the form

$$n_3(t) = 2\rho^{(1D)} \sqrt{R^2 - t^2} \Theta(R-t), \tag{C3}$$

$$n_2(t) = 2\rho^{(1D)} \frac{R}{\sqrt{R^2 - t^2}} \Theta(R-t), \tag{C4}$$

$$\mathbf{n}_{V2}(t) = \frac{(2\rho^{(1D)}t)}{\sqrt{R^2 - t^2}} \Theta(R-t) \hat{\mathbf{t}}, \tag{C5}$$

where $\Theta(x) = 1$ for $x \geq 0$ and $\Theta(x) = 0$ for $x < 0$. The 1D packing fraction is defined by $\eta = 2\rho^{(1D)}R$. Measuring length in units R , and letting $R = 1$, then the weighted densities are given by (in the cylinder: $t \leq 1$)

$$n_3(t) = \eta \sqrt{1-t^2} \Theta(1-t), \tag{C6}$$

$$n_2(t) = \frac{\eta}{\sqrt{1-t^2}} \Theta(1-t), \quad n_1(t) = \frac{\eta}{4\pi\sqrt{1-t^2}} \Theta(1-t),$$

$$n_0(t) = \frac{\eta}{4\pi\sqrt{1-t^2}} \Theta(1-t), \tag{C7}$$

$$\begin{aligned}\mathbf{n}_{V2}(t) &= \eta \frac{t}{\sqrt{1-t^2}} \Theta(1-t) \hat{\mathbf{t}}, \\ \mathbf{n}_{V1}(t) &= \frac{\eta}{4\pi} \frac{t}{\sqrt{1-t^2}} \Theta(1-t) \hat{\mathbf{t}},\end{aligned}\quad (\text{C8})$$

As a check of the weighted densities we rederived the limit for the excess free energy per particle (with $\lambda=0$) [34,43]:

$$\begin{aligned}f_{1+2}^{(1D)} &= \frac{(1/k_B T) F_{\text{ex}}[\{\rho(\mathbf{r})\}]}{N} \\ &= \frac{1}{\eta} \int_0^1 4\pi t \, dt [\Phi_1^{(3)}(t) + \Phi_2^{(3)}(t)] = -\ln(1-\eta),\end{aligned}\quad (\text{C9})$$

which is the exact 1D excess free energy. With the substitution $u = \sqrt{1-t^2}$, $t \, dt = -u \, du$, this and subsequent integrals can be calculated analytically.

The direct correlation function coefficients $\Psi_{\alpha\beta} = \Phi''_{\alpha\beta} = \partial^2 \Phi / \partial n_\alpha \partial n_\beta$ are given in Appendix A. The two-particle direct correlation function for a pair at distance r on the line ($x=0, y=0$) [r is in units of $R=1$, and recall that $c(r > 2R) = 0$] is written in the form

$$-c(r) = -c_U(r) - c_N(r), \quad (\text{C10})$$

where

$$\begin{aligned}-c_U(r) &= 4\pi \int_0^{1-r/2} dz \int_0^{r_m(z)} \Psi_{33}(t) t \, dt \\ &+ 4\pi \int_0^{1-r/2} \bar{\Psi}_{32}(t=r_m(z)) dz \\ &+ \frac{r_m(z=0) \bar{\Psi}_{12}(r_m(z=0))}{r \sqrt{1-(r/2)^2}},\end{aligned}\quad (\text{C11})$$

and

$$-c_N(r) = 4\pi \int_0^{1-r/2} \bar{\Psi}_{3,V2}(t=r_m(z)) r_m(z) dz, \quad (\text{C12})$$

and where we defined

$$r_m(z) = \sqrt{1 - \left(\frac{r}{2} + z\right)^2}, \quad (\text{C13})$$

$$\bar{\Psi}_{32}(t) = \Psi_{32}(t) + \frac{\Psi_{31}(t)}{4\pi} + \frac{\Psi_{30}(t)}{4\pi}, \quad (\text{C14})$$

$$\bar{\Psi}_{3,V2}(t) = \Psi_{3,V2}(t) + \frac{\Psi_{3,V1}(t)}{4\pi}, \quad (\text{C15})$$

$$\begin{aligned}\bar{\Psi}_{12}(r_m(z=0)) &= \Psi_{12}(r_m(z=0)) \\ &+ \Psi_{V1,V2}(r_m(z=0))(1-r^2/2).\end{aligned}\quad (\text{C16})$$

As for the 2D limit above, $c_U(r)$ contains the terms that contribute to the uniform (bulk) 3D fluid result, and $c_N(r)$ contains the remaining terms (which may contribute for the general nonuniform 3D fluid). The integrations can be performed analytically, and the result is

$$-c(r) = -c_{\text{exact}}(r) = \frac{\eta}{(1-\eta)^2} \left(1 - \frac{r}{2}\right) + \frac{1}{1-\eta}, \quad (\text{C17})$$

where $c_{\text{exact}}(r)$ is the exact 1D result. Notice the $\ln(r)$ singularity at $r=0$ in the contribution of $\bar{\Psi}_{3,V2}(t)$ and of the first two terms of $\bar{\Psi}_{3,2}(t)$ which, however, cancels out.

The contribution of the new third term, $\Phi_{3,\text{asym}(3)}^{(3D)}$, to the 1D limit excess free energy is given by

$$\begin{aligned}f_{3,\text{a sym}(3)}^{(1D)} &= \frac{1}{\eta} \int_0^1 4\pi t \, dt \Phi_{3,\text{asym}(3)}^{(3)}(t) \\ &= \frac{1}{6\eta^3} \left[\frac{10}{3} - \left(-\frac{1}{1-\eta} - 4\ln(1-\eta) \right) \right. \\ &\quad \left. + 6(1-\eta) - 2(1-\eta)^2 + \frac{1}{3}(1-\eta)^3 \right].\end{aligned}\quad (\text{C18})$$

The ratio $f_{3,\text{a sym}(3)}^{(1D)} / f_{1+2}^{(1D)}$ is small for most values of η : it is about 1/10 at $\eta=0.7$, and reaches 1 only at $\eta=0.97$ (see Fig. 15)

APPENDIX D: EXCESS FREE ENERGY OF THE 0D LIMIT

Consider hard spheres in any number of dimensions inside a cavity that cannot hold more than one particle. The exact 0D limit can be obtained as follows. The canonical partition function is Z_1 for $N=1$ and $Z_{N \geq 2} = 0$. The grand partition is

$$\Xi = \sum_{N=0}^{\infty} \frac{Z_N}{N!} e^{\beta\mu N} = 1 + Z_1 e^{\beta\mu}, \quad (\text{D1})$$

where $\beta = 1/k_B T$, from which we get

$$N = \frac{\partial}{\partial \beta\mu} \ln \Xi = \frac{Z_1 e^{\beta\mu}}{1 + Z_1 e^{\beta\mu}} \quad (\text{D2})$$

so that

$$\beta\mu = \ln \left(\frac{N}{Z_1(1-N)} \right). \quad (\text{D3})$$

The ‘pressure’ is

$$\beta P = \ln \Xi = -\ln(1-N), \quad (\text{D4})$$

so that the free energy is

$$\beta F = -\beta P + \beta\mu N = \ln(1-N) + N \ln \left[\frac{N}{Z_1(1-N)} \right]. \quad (\text{D5})$$

For ideal particles with no restriction on occupation of the cavity, and $Z_N = (Z_1)^N$, so that

$$\Xi = \exp(Z_1 e^{\beta\mu}), \quad (\text{D6})$$

$$N = Z_1 e^{\beta\mu}, \quad (\text{D7})$$

$$\beta\mu^{\text{id}} = \ln\left(\frac{N}{Z_1}\right), \quad (\text{D8})$$

$$\beta P^{\text{id}} = N, \quad (\text{D9})$$

and

$$\beta F^{\text{id}} = -N + N \ln\left(\frac{N}{Z_1}\right). \quad (\text{D10})$$

Thus the excess free energy is

$$\beta(F - F^{\text{id}}) = N + (1 - N) \ln(1 - N), \quad (\text{D11})$$

which, as the pressure, is independent of Z_1 , i.e., they correspond to the equation of state of a well-defined $D=0$ limit, which does not depend on the details of the confining potential.

APPENDIX E: FUNDAMENTAL-MEASURE WEIGHTED DENSITIES FOR A SPHERICALLY SYMMETRIC DENSITY DISTRIBUTION

Considering a spherically symmetric density distribution centered at the origin,

$$\rho(\mathbf{r}) = \rho(r), \quad (\text{E1})$$

we would like to calculate the corresponding weighted densities

$$n_\alpha(\mathbf{r}) = \int \rho(\mathbf{r}') w^{(\alpha)}(\mathbf{r} - \mathbf{r}') d\mathbf{r}', \quad (\text{E2})$$

For the scalar weights this is easily done using

$$n_\alpha(r) = \frac{2\pi}{r} \int_0^\infty w^{(\alpha)}(r') r' dr' \int_{|r-r'|}^{r+r'} \rho(y) y dy. \quad (\text{E3})$$

The vector function obtained from $\mathbf{n}_{V2}(\mathbf{r}) = -\nabla n_3(r)$. For a Gaussian density distribution centered at the origin

$$\rho(\mathbf{r}) = \eta_0 \left(\frac{\alpha}{\pi}\right)^{3/2} e^{-\alpha r^2} \quad (\text{E4})$$

then for $w^{(3)}(r') = \Theta(R - r')$ we use either Eq. (E3) or

$$n_\alpha(r) = 2\pi \int_0^\infty w^{(\alpha)}(r') r' dr' \times \int_{-r'}^{r'} \eta_0 \left(\frac{\alpha}{\pi}\right)^{3/2} e^{-\alpha(r^2+r'^2-2rz')} dz' \quad (\text{E5})$$

to get

$$n_3(r) = \frac{\eta_0}{2} \left[\text{erf}[\sqrt{\alpha}(R+r)] + \text{erf}[\sqrt{\alpha}(R-r)] + \frac{e^{-\alpha(R+r)^2} - e^{-\alpha(R-r)^2}}{r\sqrt{\alpha\pi}} \right], \quad (\text{E6})$$

which for $\alpha R^2 \gg 1$ takes the form

$$n_3(r) = \frac{\eta_0}{2} \left[1 + \text{erf}[\sqrt{\alpha}(R-r)] - \frac{e^{-\alpha(R-r)^2}}{r\sqrt{\alpha\pi}} \right]. \quad (\text{E7})$$

For $w^{(2)}(r') = \delta(R - r')$ we get

$$n_2(r) = \eta_0 \frac{R}{r} \sqrt{\frac{\alpha}{\pi}} (e^{-\alpha(R-r)^2} - e^{-\alpha(R+r)^2}) \quad (\text{E8})$$

and for $\alpha R^2 \gg 1$ it takes the form

$$n_2(r) = \eta_0 \frac{R}{r} \sqrt{\frac{\alpha}{\pi}} e^{-\alpha(R-r)^2}. \quad (\text{E9})$$

The vector function, obtained from $\mathbf{n}_{V2}(\mathbf{r}) = -\nabla n_3(r)$, is given by

$$\frac{\mathbf{n}_{V2}(\mathbf{r})}{n_2(r)} = \boldsymbol{\xi}(\mathbf{r}) = \left(\frac{1 + e^{-4\alpha r R}}{1 - e^{-4\alpha r R}} - \frac{1}{2\alpha r R} \right) \frac{\mathbf{r}}{r}. \quad (\text{E10})$$

- [1] For a recent review, see *Density Functional Theory*, Vol. 337 of *NATO Advanced Study Institute, Series B: Physics*, edited by E.K.U. Gross and R.M. Drexlner (Plenum Press, New York, 1995).
- [2] H. Löwen, *Phys. Rep.* **237**, 249 (1994).
- [3] See the recent collection of reviews, *Fundamentals of Inhomogeneous Fluids*, edited by D. Henderson (Dekker, New York, 1992), and in particular the review by R. Evans.
- [4] J.P. Hansen and I.R. McDonald, *Theory of Simple Liquids*, 2nd ed. (Academic Press, London, 1986).
- [5] B.K. Peterson, K. Gubbins, G.S. Heffelfinger, U. Marini Bettolo Marconi, and F. van Swol, *J. Chem. Phys.* **88**, 6487 (1988).

- [6] *Molecular Dynamics in Restricted Geometries*, edited by J. Klafter and J.M. Drake (John Wiley, New York, 1989).
- [7] H.K. Christenson, *Phys. Rev. Lett.* **74**, 4675 (1995).
- [8] M. Schmidt and H. Löwen, *Phys. Rev. Lett.* **76**, 4522 (1996); Martin Schoen *et al.*, *J. Chem. Phys.* **101**, 6865 (1994).
- [9] See, for example, T. Fehr and H. Löwen, *Phys. Rev. E* **52**, 4016 (1995).
- [10] M. Krech, *The Casimir Effect in Critical Systems* (World Scientific, Singapore, 1995).
- [11] J.A. Duffy, N.J. Wilkinson, H.M. Fretwell, M.A. Alam, and R. Evans, *J. Phys. Condens. Matter* **7**, L713 (1995).
- [12] P. Pieranski, L. Strzelcki, and B. Pansu, *Phys. Rev. Lett.* **50**, 900 (1983).

- [13] D.H. van Winkle and C.A. Murray, *Phys. Rev. A* **34**, 562 (1986); C.A. Murray, W.O. Sprenger, and R.A. Wenk, *Phys. Rev. B* **42**, 688 (1990); C.A. Murray, in *Bond-Orientational Order in Condensed Matter Systems*, edited by K.J. Strandburg (Springer, New York, 1992).
- [14] G. Martinelli Kepler and S. Fraden, *Langmuir* **10**, 2501 (1994).
- [15] J. Weis, D.W. Oxtoby, D.G. Grier, and C.A. Murray, *J. Chem. Phys.* **103**, 1180 (1995).
- [16] J.C. Crocker and D.G. Grier, *Phys. Rev. Lett.* **73**, 352 (1994).
- [17] G. Martinelli Kepler and S. Fraden, *Phys. Rev. Lett.* **73**, 356 (1994).
- [18] D.G. Grier and C.A. Murray, *J. Chem. Phys.* **100**, 9088 (1994).
- [19] G. Rodriguez and L. Vicente, *Mol. Phys.* **87**, 213 (1996).
- [20] C.N. Patra and S.K. Ghosh, *Phys. Rev.* **50**, 5123 (1994).
- [21] J.E. Hug, F. van Swol, and C.F. Zukowski, *Langmuir* **11**, 111 (1995).
- [22] J.K. Percus, *J. Stat. Phys.* **23**, 657 (1980).
- [23] M.S. Wertheim, L. Blum, and D. Bratko, in *Micellar Solutions and Microemulsions: Structure, Dynamics, and Statistical Thermodynamics*, edited by S.-H. Chen and R. Rajagopalan (Springer, New York, 1990).
- [24] T. Biben, R. Ohnesorge, and H. Löwen, *Europhys. Lett.* **28**, 665 (1994).
- [25] J.K. Percus, *J. Stat. Phys.* **15**, 505 (1976).
- [26] J.K. Percus, *J. Stat. Phys.* **52**, 1157 (1988).
- [27] P. Tarazona, *Mol. Phys.* **52**, 81 (1984); *Phys. Rev. A* **31**, 2672 (1985).
- [28] See, e.g., the review by M. Baus, *J. Phys. Condens. Matter* **2**, 2241 (1990).
- [29] R. Ohnesorge, H. Löwen, and H. Wagner, *Europhys. Lett.* **22**, 245 (1993); *Phys. Rev. E* **50**, 4801 (1994).
- [30] Y. Rosenfeld, in *Chemical Applications of Density-Functional Theory*, edited by B. Laird, R. Ross, and T. Ziegler, ACS Symposium Series Vol. 629 (American Chemical Society, Washington, DC, 1996), pp. 198–211; in *Strongly Coupled Plasma Physics*, edited by W. Kraeft and M. Schlanges (World Scientific, Singapore, 1996), pp. 27–36; *J. Phys. Condens. Matter* **8**, 9289 (1996).
- [31] Y. Rosenfeld, *Phys. Rev. Lett.* **63**, 980 (1989); *J. Chem. Phys.* **93**, 4305 (1990); Y. Rosenfeld, D. Levesque, and J.J. Weis, *ibid.* **92**, 6818 (1990).
- [32] Y. Rosenfeld, *Phys. Rev. E* **50**, R3318 (1994); *Mol. Phys.* **86**, 637 (1995).
- [33] Y. Rosenfeld, *Phys. Rev. A* **42**, 5978 (1990).
- [34] Y. Rosenfeld, *J. Chem. Phys.* **98**, 8126 (1993); *Phys. Rev. E* **54**, 2827 (1996).
- [35] Y. Rosenfeld, *Phys. Rev. Lett.* **72**, 3831 (1994); *J. Phys. Chem.* **99**, 2857 (1995).
- [36] Y. Rosenfeld, M. Schmidt, H. Löwen, and P. Tarazona, *J. Phys. Condens. Matter* **8**, L577 (1996).
- [37] Y. Rosenfeld, *Phys. Rev. A* **32**, 1834 (1985); **33**, 2025 (1986); *Phys. Rev. E* **47**, 2676 (1993), and references therein.
- [38] Y. Rosenfeld and N.W. Ashcroft, *Phys. Rev. A* **20**, 1208 (1979).
- [39] Y. Rosenfeld, *J. Chem. Phys.* **89**, 4272 (1988).
- [40] J.K. Percus and G.J. Yeveick, *Phys. Rev.* **110**, 1 (1958); J.L. Lebowitz, *Phys. Rev. A* **133**, 895 (1964).
- [41] H. Reiss, H. Frisch, and J.L. Lebowitz, *J. Chem. Phys.* **31**, 369 (1959); H. Reiss, *J. Phys. Chem.* **96**, 4736 (1992).
- [42] E. Kierlik and M.L. Rosinberg, *Phys. Rev. A* **42**, 3382 (1990).
- [43] E. Kierlik and M.L. Rosinberg, *Phys. Rev. A* **44**, 5025 (1991); and private communication.
- [44] S. Phan, E. Kierlik, M.L. Rosinberg, B. Bildstein, and G. Kahl, *Phys. Rev. E* **48**, 618 (1993).
- [45] J. Jung, M.S. Jhon, and F. Ree, *J. Chem. Phys.* **100**, 528 (1994); **100**, 9064 (1994).
- [46] K. Swamy independently confirmed the $1/r$ singularity.
- [47] F. Lado, *J. Chem. Phys.* **49**, 3092 (1968).
- [48] Gaussians can be considered numerically as strictly confined only for relatively large values of α , but certainly for values which are relevant for describing the solid.
- [49] P. Tarazona (unpublished).
- [50] Y. Rosenfeld, *J. Phys. Condens. Matter* **8**, L795 (1996).
- [51] For example, for classical plasmas of point charges in a uniform background pair correlation functions were obtained with $\Phi_3^{(3)}$ which are almost indistinguishable from the simulation results, and the energies agree to better than 0.1% (see Ref. [34] above). Yet the inverse compressibility, as obtained from integrating the direct correlation functions, deviates from that obtained from differentiating the energy equation of state by as much as 30% near freezing densities. With the new $\Phi_{3,\text{asym}(3)}^{(3)}$ similarly accurate results for the pair correlations are obtained, but this deviation is now reduced to only about 10% [Y. Rosenfeld (unpublished)]. In the case of the Lennard-Jones system both $\Phi_3^{(3)}$ and $\Phi_{3,\text{asym}(3)}^{(3)}$ yield pressures, energies, and inverse compressibilities *all* in about 1% agreement with the simulation data, yet the results using $\Phi_3^{(3)}$ are slightly better [Y. Rosenfeld (unpublished)]. It was found [Y. Rosenfeld and G. Kahl, *J. Phys. Condens. Matter* **9**, L89 (1997)] that using $\Phi_{3,\text{asym}(3)}^{(3)}$ instead of $\Phi_3^{(3)}$ hardly affects the properties of the functional in applications to the inverse scattering problem as discussed in Ref. [56].
- [52] M. Schmidt and H. Löwen (unpublished).
- [53] J.A. Cuesta, *Phys. Rev. Lett.* **76**, 3742 (1996).
- [54] A. Santos, M. Lopez de Haro, and S. Bravo Yuste, *J. Chem. Phys.* **103**, 4622 (1995).
- [55] W.G. Hoover and F.H. Ree, *J. Chem. Phys.* **49**, 3609 (1968); B.J. Alder, W.G. Hoover, and D.A. Young, *ibid.* **49**, 3688 (1968); D.A. Young and B.J. Alder, *ibid.* **60**, 1254 (1974).
- [56] G. Kahl, B. Bildstein, and Y. Rosenfeld, *Phys. Rev. E* **54**, 5391 (1996).